

Diverse properties of Ly α emission in low-redshift compact star-forming galaxies with extremely high [O III]/[O II] ratios

Y. I. Izotov^{1,2}, D. Schaerer^{3,4}, G. Worseck⁵, A. Verhamme³, N. G. Guseva^{1,2},
T. X. Thuan⁶, I. Orlitová⁷ & K. J. Fricke^{8,2}

¹*Bogolyubov Institute for Theoretical Physics, National Academy of Sciences of Ukraine, 14-b Metrolohichna str., Kyiv, 03143, Ukraine,*
E-mail: yizotov@bitp.kiev.ua, nguseva@bitp.kiev.ua

²*Max-Planck-Institut für Radioastronomie, Auf dem Hügel 69, 53121 Bonn, Germany*

³*Observatoire de Genève, Université de Genève, 51 Ch. des Maillettes, 1290, Versoix, Switzerland,*
E-mail: daniel.schaerer@unige.ch, anne.verhamme@unige.ch

⁴*IRAP/CNRS, 14, Av. E. Belin, 31400 Toulouse, France*

⁵*Institut für Physik und Astronomie, Universität Potsdam, Karl-Liebknecht-Str. 24/25, D-14476 Potsdam, Germany,*
E-mail: gworseck@uni-potsdam.de

⁶*Astronomy Department, University of Virginia, P.O. Box 400325, Charlottesville, VA 22904-4325, USA,*
E-mail: txt@virginia.edu

⁷*Astronomical Institute, Czech Academy of Sciences, Boční II 1401, 141 00, Prague, Czech Republic,*
E-mail: orlitova@asu.cas.cz

⁸*Institut für Astrophysik, Göttingen Universität, Friedrich-Hund-Platz 1, 37077 Göttingen, Germany,*
E-mail: kfricke@gwdg.de

Accepted XXX. Received YYY; in original form ZZZ

ABSTRACT

We present observations with the Cosmic Origins Spectrograph onboard the *Hubble Space Telescope* of eight compact star-forming galaxies at redshifts $z = 0.02811 - 0.06540$, with low oxygen abundances $12 + \log(\text{O}/\text{H}) = 7.43 - 7.82$ and extremely high emission-line flux ratios $\text{O}_{32} = [\text{O III}]\lambda 5007/[\text{O II}]\lambda 3727 \sim 22 - 39$, aiming to study the properties of Ly α emission in such conditions. We find a diversity in Ly α properties. In five galaxies Ly α emission line is strong, with equivalent width (EW) in the range 45 – 190 Å. In the remaining galaxies, weak Ly α emission with $\text{EW}(\text{Ly}\alpha) \sim 2 - 7 \text{ \AA}$ is superposed on a broad Ly α absorption line, indicating a high neutral hydrogen column density $N(\text{H I}) \sim (1 - 3) \times 10^{21} \text{ cm}^{-2}$. We examine the relation between the Ly α escape fraction $f_{\text{esc}}(\text{Ly}\alpha)$ and the Lyman continuum escape fraction $f_{\text{esc}}(\text{LyC})$, using direct measures of the latter in eleven low-redshift LyC leakers, to verify whether $f_{\text{esc}}(\text{Ly}\alpha)$ can be an indirect measure of escaping LyC radiation. The usefulness of O_{32} , of the Ly α equivalent width $\text{EW}(\text{Ly}\alpha)$ and of the Ly α peak separation V_{sep} as indirect indicators of Ly α leakage is also discussed. It is shown that there is no correlation between O_{32} and $f_{\text{esc}}(\text{Ly}\alpha)$. We find an increase of $f_{\text{esc}}(\text{Ly}\alpha)$ with increasing $\text{EW}(\text{Ly}\alpha)$ for $\text{EW}(\text{Ly}\alpha) < 100 \text{ \AA}$, but for higher $\text{EW}(\text{Ly}\alpha) \gtrsim 150 \text{ \AA}$ the $f_{\text{esc}}(\text{Ly}\alpha)$ is nearly constant attaining the value of ~ 0.25 . We find an anticorrelation between $f_{\text{esc}}(\text{Ly}\alpha)$ and V_{sep} , though not as tight as the one found earlier between $f_{\text{esc}}(\text{LyC})$ and V_{sep} . This finding makes V_{sep} a promising indirect indicator of both the Ly α and ionizing radiation leakage.

Key words: (cosmology:) dark ages, reionization, first stars — galaxies: abundances — galaxies: dwarf — galaxies: fundamental parameters — galaxies: ISM — galaxies: starburst

1 INTRODUCTION

The extremely high $\text{O}_{32} = [\text{O III}]\lambda 5007/[\text{O II}]\lambda 3727$ ratio in spectra of low-redshift dwarf star-forming galaxies (SFGs)

indicates the presence of either an ionization-bounded compact H II region with intense ionizing radiation from a very young star-forming region or a density-bounded H II region losing its ionizing radiation, or both (e.g. Jaskot & Oey 2013; Nakajima & Ouchi 2014; Stasińska et al. 2015; Izotov et al. 2017). The ionizing photon production efficiency $\xi_{\text{ion}} = N_{\text{LyC}}/L_{\nu}$ in these galaxies could be very high, where N_{LyC} is the Lyman continuum photon production rate and L_{ν} is the monochromatic UV luminosity at $\lambda = 1500\text{\AA}$. Therefore, they are considered as the local counterparts of the dwarf SFGs at high redshifts, which are likely the main source of the last phase transition of the matter in the Universe, namely its reionization, which ends at $z \sim 6$ (Ouchi et al. 2009; Wise & Chen 2009; Kashikawa et al. 2011; Jiang et al. 2013; Mitra, Ferrara & Choudhury 2013; Yajima, Choi & Nagamine 2011; Bouwens et al. 2015; Smith et al. 2018; Naidu et al. 2018; Steidel et al. 2018; Kimm et al. 2019). An alternative hypothesis is the dominant role of active galactic nuclei (AGN) in the reionization of the Universe, as proposed e.g. by Madau & Haardt (2015). However, in recent years, growing evidence for a small contribution of AGN to reionization has accumulated (e.g. Hassan et al. 2018; Mitra, Choudhury & Ferrara 2018; Parsa, Dunlop & McLure 2018; Matsuoka et al. 2018; Kulkarni, Worseck & Hennawi 2019). On the other hand, SFGs can be considered as an important source of ionization only if the product $\xi_{\text{ion}} \times f_{\text{esc}}(\text{LyC})$ is sufficiently high, where $f_{\text{esc}}(\text{LyC})$ is the escape fraction of Lyman continuum (LyC), i.e. the fraction of ionizing radiation emitted into the intergalactic medium (IGM). It has been estimated that $f_{\text{esc}}(\text{LyC})$ should not be less than 10–20 per cent on average in order to accomplish reionization (e.g. Ouchi et al. 2009; Robertson et al. 2013; Dressler et al. 2015; Robertson et al. 2015; Khaire et al. 2016).

Currently, direct observations of the LyC are available for only a limited number of galaxies at high and low redshifts. Searches for and confirmation of LyC emission from high redshift galaxies are difficult due to their faintness, contamination by lower-redshift interlopers and attenuation by residual H I in the highly ionized IGM. (e.g., Vanzella et al. 2010, 2012; Inoue et al. 2014; Grazian et al. 2016). They have resulted in the discovery of approximately three dozens of LyC leakers with reliably high escape fraction: *Ion2* (Vanzella et al. 2015; de Barros et al. 2016), Q1549-C25 (Shapley et al. 2016), A2218-Flanking (Bian et al. 2017), *Ion3* (Vanzella et al. 2018), SunBurst Arc (Rivera-Thorsen et al. 2019), 15 SFGs studied by Steidel et al. (2018), and a dozen of galaxies at $z = 3.1$ with strong [O III] $\lambda 5007$ emission (Fletcher et al. 2019).

At low redshifts, $z \sim 0.3 - 0.4$, Izotov et al. (2016a,b, 2018a,b) have detected LyC leaking emission in eleven compact SFGs with high $O_{32} \sim 5 - 28$ and derived $f_{\text{esc}}(\text{LyC})$ ranging between 2 and 72 per cent. These values are higher than $f_{\text{esc}}(\text{LyC})$ of $\lesssim 1$ per cent derived by Borthakur et al. (2014) and Chisholm et al. (2017) in SFGs with lower O_{32} , or by Hernandez et al. (2018) in SFGs with lower equivalent widths of the H β emission line. There is hope that the number of low- z LyC leakers will considerably be increased after the completion in 2020 of the *HST* Large Program GO 15626 (P.I. A. Jaskot), which includes more than 70 targets.

The *Hubble Space Telescope* (*HST*)/Cosmic Origins Spectrograph (COS) sensitivity curve limits LyC observations to $z \gtrsim 0.25$. At lower redshifts, only very bright targets

are accessible (e.g. Leitherer et al. 2016). Therefore, for low-redshift SFGs, reliable indirect indicators of LyC leakage are needed. Nakajima & Ouchi (2014) proposed that high O_{32} can be an indication of density-bounded H II region and thus of LyC leakage. However, O_{32} depends on some other parameters, such as ionization parameter and hardness of radiation which in turn depend on metallicity.

Faisst (2016) has found a correlation between $f_{\text{esc}}(\text{LyC})$ and O_{32} , using a small sample of galaxies which includes low- z LyC leakers with $O_{32} < 8$. On the other hand, no correlation has been found by Izotov et al. (2018b) for eleven confirmed LyC leakers with O_{32} in a wide range of $\sim 5 - 28$. A similar conclusion was obtained by Naidu et al. (2018) and Bassett et al. (2019) (see also Rutkowski et al. 2017). However, this conclusion is based mainly on observations of galaxies with $O_{32} \lesssim 16$. Only one observed galaxy has a higher value of O_{32} . It is thus important to observe LyC emission in more galaxies with higher O_{32} .

The He I emission-line ratios in optical spectra of galaxies can also be used to estimate the column density of neutral gas and thus to indirectly estimate $f_{\text{esc}}(\text{LyC})$ (Izotov et al. 2017). However, deep spectra in the optical range are needed since these lines are weak with intensities $\lesssim 10$ per cent of the H β emission line.

Finally, the properties of the Ly α emission line can serve as indirect indicators of escaping LyC emission. Its profile is double-peaked in the spectra of most of LyC leakers, with the separation between the peaks V_{sep} decreasing with decreasing neutral hydrogen column density $N(\text{H I})$ (e.g. Izotov et al. 2016a,b, 2018a,b). In rare cases, the Ly α profile is more complex and consists of three and more peaks (Rivera-Thorsen et al. 2017; Izotov et al. 2018b; Vanzella et al. 2018). Verhamme et al. (2015) and Izotov et al. (2018b) have shown that there is a tight relation between the LyC escape fraction $f_{\text{esc}}(\text{LyC})$ and the separation between Ly α peaks, making V_{sep} the most reliable indicator of escaping ionizing radiation. Furthermore, Verhamme et al. (2017) have shown for a limited sample of LyC leakers that the Ly α escape fractions $f_{\text{esc}}(\text{Ly}\alpha)$ are larger than the LyC escape fractions $f_{\text{esc}}(\text{LyC})$, in accord with theoretical predictions of Dijkstra, Gronke & Venkatesan (2016).

In this paper we present new *HST*/COS observations of the Ly α in eight low-redshift ($z < 0.07$) compact SFGs with the highest $O_{32} \sim 22 - 39$ found in the Sloan Digital Sky Survey (SDSS), aiming to examine the properties of Ly α emission in these galaxies and to verify possible indirect indicators of escaping Ly α and LyC emission. The studied galaxies have lower stellar masses than previously observed Ly α emitting galaxies such as the “green pea” (GP) galaxies at $z \sim 0.1 - 0.3$ studied e.g. by Jaskot et al. (2017), Yang et al. (2017a), McKinney et al. (2019), and the confirmed LyC leakers at $z \sim 0.3 - 0.4$ (Izotov et al. 2016a,b, 2018a,b). The selection criteria and the properties of the selected galaxies derived from observations in the optical range are presented in Section 2. The *HST* observations and data reduction are described in Section 3. The surface brightness profiles in the UV range are discussed in Section 4. Ly α emission is considered in Section 5. In Section 6, our results are compared with the Ly α escape fractions obtained for other galaxies in some recent studies. We summarize our findings in Section 7.

Table 1. Some general characteristics of the selected galaxies from the SDSS data base

Name	R.A.(2000.0)	Dec.(2000.0)	z	D_L^a (Mpc)	D_A^b (Mpc)	O_{32}^c	EW(H β) (\AA)	FWHM ^d (arcsec)	12+log(O/H) ^e
J0007+0226	00:07:24.49	+02:26:27.20	0.06360	287	254	35	258	1.18	7.82
J0159+0751	01:59:52.75	+07:51:48.80	0.06105	275	245	39	322	1.05	7.56
J0820+5431	08:20:19.27	+54:31:40.10	0.03851	171	158	22	334	1.29	7.49
J0926+4504	09:26:55.44	+45:04:32.30	0.04232	188	173	22	328	1.42	7.68
J1032+4919	10:32:56.72	+49:19:47.24	0.04420	197	181	24	444	1.27	7.59
J1205+4551	12:05:03.55	+45:51:50.94	0.06540	296	261	23	483	1.37	7.44
J1242+4851	12:42:26.46	+48:51:57.67	0.06226	281	249	25	360	1.25	7.43
J1355+4651	13:55:25.66	+46:51:51.34	0.02811	124	117	23	269	1.35	7.56

^aLuminosity distance (NED, [Wright 2006](#)).

^bAngular size distance (NED, [Wright 2006](#)).

^c $O_{32} = [\text{O III}]\lambda 5007 / [\text{O II}]\lambda 3727$. For J1032+4919, $O_{32} = 3 \times [\text{O III}]\lambda 4959 / [\text{O II}]\lambda 3727$.

^dFull width at half maximum in the SDSS g -band image.

^eOxygen abundance derived from line intensities in the SDSS spectrum.

Table 2. Apparent magnitudes with errors in parentheses compiled from the SDSS, *GALEX*^a and *WISE*^b databases

Name	SDSS (AB)					GALEX (AB)		WISE (Vega)			
	u (err)	g (err)	r (err)	i (err)	z (err)	FUV (err)	NUV (err)	W1 (err)	W2 (err)	W3 (err)	W4 (err)
J0007+0226	21.06 (0.13)	19.73 (0.02)	20.66 (0.05)	19.82 (0.03)	20.44 (0.23)	21.80 (0.31)	21.28 (0.22)	17.40 (0.19)	17.03 (0.50)	11.92 (0.32)	...
J0159+0751	20.67 (0.11)	19.47 (0.02)	20.36 (0.05)	19.57 (0.04)	19.89 (0.18)	21.21 (0.27)	20.43 (0.29)	17.39 (0.15)	15.88 (0.15)	11.54 (0.19)	8.52 (0.30)
J0820+5431	21.44 (0.13)	20.41 (0.02)	21.55 (0.09)	21.44 (0.12)	21.47 (0.51)	21.67 (0.34)	21.59 (0.24)	16.52 (0.07)	16.59 (0.25)
J0926+4504	21.10 (0.11)	19.92 (0.02)	21.11 (0.08)	20.68 (0.07)	20.54 (0.23)	22.12 (0.44)	21.74 (0.32)	...	17.26 (0.48)	12.37 (0.44)	...
J1032+4919	19.89 (0.04)	18.67 (0.01)	20.01 (0.02)	19.60 (0.02)	20.15 (0.15)	20.26 (0.20)	20.25 (0.14)	16.60 (0.08)	15.08 (0.07)	10.50 (0.07)	7.74 (14)
J1205+4551	20.52 (0.05)	19.79 (0.01)	20.98 (0.04)	19.61 (0.02)	20.80 (0.16)	21.04 (0.34)	20.58 (0.19)	15.14 (0.04)	13.55 (0.03)	9.91 (0.05)	7.80 (0.19)
J1242+4851	21.30 (0.09)	20.35 (0.02)	21.51 (0.07)	20.56 (0.05)	21.25 (0.31)	21.36 (0.17)	21.36 (0.14)	18.37 (0.33)
J1355+4651	20.37 (0.05)	19.22 (0.01)	20.06 (0.02)	20.47 (0.05)	20.53 (0.20)	20.54 (0.23)	20.66 (0.19)	17.86 (0.19)	17.39 (0.47)

^a<http://galex.stsci.edu/GR6/>

^b<https://irsa.ipac.caltech.edu/cgi-bin/Gator/nph-dd>

2 SELECTION CRITERIA AND THE INTEGRATED PROPERTIES OF SELECTED GALAXIES

Our galaxies were selected from the SDSS Data Release 14 (DR14) ([Abolfathi et al. 2018](#)). We adopted the following selection criteria for each galaxy:

1) it has a very high $O_{32} > 20$, which is an indication of either a density-bounded H II region or a high ionization parameter.

2) it has a compact structure in the SDSS image in order to observe the total flux of the galaxy with the small 2.5 arcsec COS aperture.

3) it is isolated from other sources to avoid contamination in the *HST*/COS spectra.

4) it is sufficiently bright in the UV range (*GALEX* NUV magnitude brighter than 22 mag) to be acquired with COS.

In total, we selected the 8 brightest galaxies satisfying the above conditions.

The SDSS spectra of the selected galaxies reveal considerably lower oxygen abundances, in the range $12 + \log(\text{O}/\text{H}) = 7.43 - 7.82$ (see below), as compared to the confirmed LyC leakers ([Izotov et al. 2016a,b, 2018a,b](#)). They show comparably high rest-frame equivalent widths $\text{EW}(\text{H}\beta) = 258 - 483 \text{ \AA}$ (Table 1), indicating very recent star formation.

These galaxies are located at the extreme upper tip of the SFG branch in the Baldwin-Phillips-Terlevich (BPT) diagram (filled circles in Fig. 2a) implying the presence of high-excitation H II regions. They are considerably more extreme than the confirmed LyC leakers shown by open circles. It is seen in Fig. 2b, which shows the $O_{32} - R_{23}$ diagram, that the selected SFGs (filled circles) have the highest O_{32} ratios among all SDSS SFGs, and that they are offset to low R_{23} values compared to the main sequence of SFGs (grey dots) because of their lower metallicities. On the other hand, most of the confirmed LyC leakers with higher metallicities are located in the upper part of the main sequence (open circles).

The SDSS spectra were used to derive the interstellar



Figure 1. 12 arcsec \times 12 arcsec SDSS composite images of galaxies with extreme O_{32} ratios observed with the *HST*.

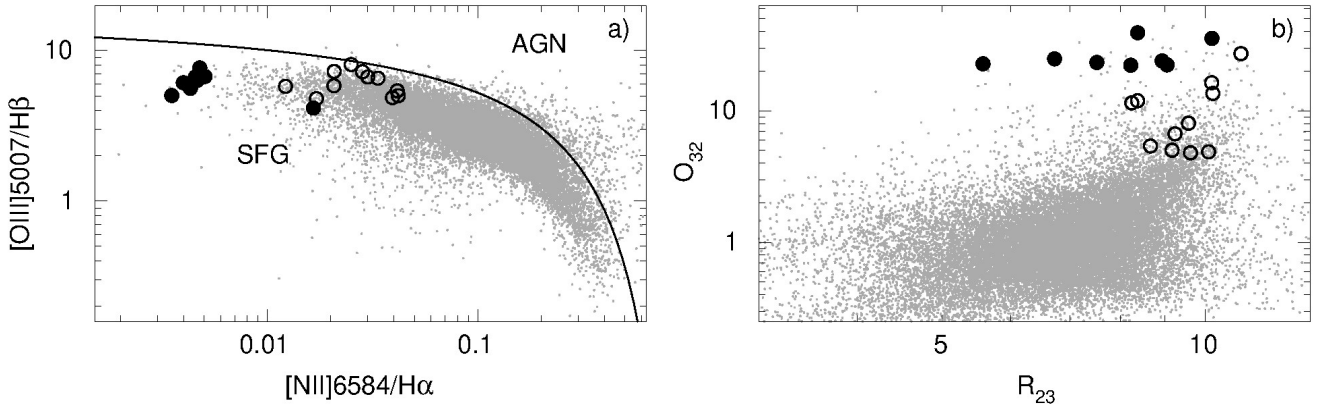


Figure 2. **a)** The Baldwin-Phillips-Terlevich (BPT) diagram (Baldwin et al. 1981) for SFGs. **b)** The $O_{32} - R_{23}$ diagram for SFGs where $R_{23} = ([O II]\lambda 3727 + [O III]\lambda 4959 + [O III]\lambda 5007)/H\beta$. In both panels, the galaxies from this paper and LyC leaking galaxies (Izotov et al. 2016a,b, 2018a,b) are shown by filled circles and open circles, respectively. The compact SFGs from the SDSS (Izotov et al. 2016c) are represented by grey dots. The solid line in **a)** by Kauffmann et al. (2003) separates SFGs from active galactic nuclei (AGN).

extinction from the hydrogen Balmer decrement and ionized gas metallicity using the prescriptions of Izotov, Thuan & Lipovetsky (1994), Izotov et al. (2006) and Guseva et al. (2013).

The extinction-corrected emission-line flux densities, the extinction coefficients $C(H\beta)$, the rest-frame equivalent widths of $H\beta$, $[O III]\lambda 5007$ and $H\alpha$ emission lines, and the observed $H\beta$ flux densities are shown in Table A1. We note that the $H\alpha$ emission line in the SDSS spectra of J0820+5431 and J1032+4919 and the $[O III]\lambda 5007$ emission line in the SDSS spectrum of J1032+4919 are clipped. Therefore, for J1032+4919, $I([O III]\lambda 5007) = 3 \times I([O III]\lambda 4959)$ is used to derive O_{32} , the electron temperature $T_e(O III)$ and oxygen abundance. Furthermore, the $H\alpha$ emission line in this galaxy and in J0820+5431 is excluded in the calculation of extinc-

tion. The $He II \lambda 4686 \text{ \AA}$ emission line is detected in seven out of eight galaxies implying hard ionizing radiation.

The flux densities from Table A1 and the direct T_e method are used to derive the electron temperature, electron number density and the element abundances in the H II regions. These quantities are shown in Table A2. The oxygen abundances of our galaxies are on average $\sim 0.2 - 0.3$ dex lower than those in known low-redshift LyC leakers (Izotov et al. 2016a,b, 2018a,b). Four galaxies from our sample have been observed with the Large Binocular Telescope (LBT) by Izotov et al. (2017). Those authors derived oxygen abundances that are in good agreement with the present determinations from SDSS spectra. The neon, sulfur and argon to oxygen abundance ratios (Fig. 3) are similar to those in dwarf emission-line galaxies (e.g. Izotov et al. 2006; Guseva et al. 2013) and in confirmed LyC leakers, with similar small

dispersions. On the other hand, the N/O ratios are scattered over a large range (Fig. 3a) which can not be explained by N/O errors (Table A2). Compared to SDSS SFGs (shown by grey dots), they tend to have systematically higher values both for the galaxies in our sample and for the confirmed LyC leakers.

The emission-line luminosities and stellar masses of our galaxies were obtained adopting a luminosity distance (NED, Wright 2006) with the cosmological parameters $H_0=67.1$ km s $^{-1}$ Mpc $^{-1}$, $\Omega_\Lambda=0.682$, $\Omega_m=0.318$ (Ade et al. 2014). Using these parameters and apparent magnitudes, we also derived absolute magnitudes M_g and M_{FUV} in the SDSS g and GALEX FUV bands (Table 3), assuming negligible bandpass corrections and neglecting dust extinction.

The H β luminosity $L(H\beta)$ and corresponding star-formation rates SFR shown in Table 3 were obtained from the extinction-corrected H β flux densities using the relation by Kennicutt (1998) and adopting the value of 2.75 for the H α /H β flux ratio. They are one order of magnitude lower than the respective values for LyC leakers. Specific star formation rates sSFR = SFR/ M_\star of ~ 100 Gyr $^{-1}$ are similar to sSFRs for LyC leakers (Izotov et al. 2016a,b, 2018a,b) and are among the highest known for GPs and luminous compact galaxies (Cardamone et al. 2009; Izotov, Guseva & Thuan 2011), and dwarf SFGs at $z < 1$ (Izotov et al. 2016c). On the other hand, they are several orders of magnitude higher than the sSFRs of $\sim 0.01 - 1$ Gyr $^{-1}$ of the SDSS main sequence galaxies.

The extinction-corrected SDSS spectra of our galaxies were used to fit the spectral energy distribution (SED) of both the stellar and nebular components and to derive their stellar masses, starburst ages and the modelled intrinsic absolute magnitudes M_{FUV}^{SED} in the FUV range. The fitting method, using a two-component model, is described in Izotov et al. (2018a). We find that the stellar masses and FUV luminosities of our galaxies are ~ 2 orders of magnitude lower compared to the confirmed LyC leakers (Table 3), but their extinction-corrected absolute FUV magnitudes are similar to those of the faintest detected galaxies at $z = 6 - 8$ (e.g. Livermore, Finkelstein & Lotz 2017; Bouwens et al. 2017b).

3 HST/COS OBSERVATIONS AND DATA REDUCTION

HST/COS spectroscopy of the eight galaxies was obtained in program GO 15136 (PI: Y. I. Izotov) during the period January 2018 – February 2019. The observational details are presented in Table 4. The galaxies were acquired by COS near ultraviolet (NUV) imaging. Since our targets are compact but faint, as based on shallow GALEX imaging, a considerable fraction of one orbit was spent per object for deep NUV imaging and reliable acquisition. The NUV-brightest region of each target was centered in the 2.5 arcsec diameter spectroscopic aperture (Fig. 4). We note that acquisition observations failed for J1242+4851. We do not know the reason for that. The acquisition image has a flag raised in the header: EXPFLAG=‘INVALID CHECK IMAGE’. Possibly, something went wrong during one of the two acquisition exposures. Therefore, the imaging data for J1242+4851 are not present in this paper. However, the spectroscopic observations were not affected. For the other galaxies, some struc-

ture with an extended low-surface-brightness (LSB) component is seen. However, their sizes are smaller than the central unvignetted 0.8 arcsec diameter region of the spectroscopic aperture. Hence, the galaxy quantities derived from the COS spectra here do not require corrections for vignetting. In fact, most of the NUV continuum in these galaxies is concentrated in much smaller central regions, with full widths at half maximum $\lesssim 0.1$ arcsec.

We obtained spectra of the Ly α emission lines with the COS G130M grating positioned at the central wavelength 1222 Å and a small wavelength coverage of ~ 300 Å at COS Detector Lifetime Position 4, yielding a spectral resolving power $\lambda/\Delta\lambda \approx 14,000$ in the wavelength range of interest. All four focal-plane offset positions were employed to correct grid wire shadows and detector blemishes.

The individual exposures were reduced with the CAL-COS pipeline v3.3.4, followed by accurate background subtraction and co-addition with custom software (Worseck et al. 2016). Apart from adjustments of the rectangular extraction aperture due to the wide spatial profile of the G130M 1222 Å setup (57 pixels) and adjustments in the detector pulse-height thresholds to reflect the current detector state, the reduction procedures were analogous to Izotov et al. (2016a). We verified in the two-dimensional spectra that the extraction aperture contains all visible Ly α flux and preserves the spectrophotometry of the continuum. The estimated background uncertainties of a few per cent do not affect our analysis. The homogeneous reduction enables a fair comparison to our previous results (Izotov et al. 2016a,b, 2018a,b).

4 SURFACE BRIGHTNESS DISTRIBUTION IN THE NUV RANGE

Using the COS NUV acquisition images and the routine *ellipse* in IRAF¹/STSDAS² we obtain the surface brightness (SB) profiles of our galaxies in the UV continuum. The GALEX NUV magnitudes were used to express the profiles in the units mag arcsec $^{-2}$. For this, we have scaled the total NUV flux of the galaxy measured in the acquisition image to the flux corresponding to the GALEX NUV magnitude. The shape of the SB profiles (Fig. 5) in our galaxies is similar to those of confirmed LyC leakers (Izotov et al. 2016a,b, 2018a,b) with a sharp increase in the central part because of the presence of the bright star-forming region(s) and a linear decrease (in magnitudes) in the outer part, reminiscent of a disc structure.

However, the scale lengths α of our galaxies in the range $\sim 0.09 - 0.48$ kpc (Fig. 5) are considerably lower than $\alpha = 0.6 - 1.8$ kpc in LyC leakers (Izotov et al. 2016a,b, 2018a,b), presumably because of their considerably lower stellar masses. The scale lengths of our galaxies are among the lowest found for local blue compact dwarf galaxies (Papaderos et al.

¹ IRAF is distributed by the National Optical Astronomy Observatories, which are operated by the Association of Universities for Research in Astronomy, Inc., under cooperative agreement with the National Science Foundation.

² STSDAS is a product of the Space Telescope Science Institute, which is operated by AURA for NASA.

Table 3. Integrated characteristics

Name	$M_{\text{FUV}}^{\text{SED}^a}$	M_{FUV}^b	M_g^c	$\log M_\star^d$	SB age ^e	$\log L(\text{H}\beta)^f$	SFR ^g	$\log \xi_{\text{ion}}^h$	α^i	r_{50}^j	Σ_1^k	Σ_2^l
J0007+0226	-17.35	-15.49	-17.62	7.9	1.3	40.71	1.4	25.44	0.48	0.070	1.9	90
J0159+0751	-17.16	-15.99	-18.02	8.6	0.5	40.92	2.3	25.76	0.17	0.060	25.3	203
J0820+5431	-15.68	-14.49	-15.75	6.0	3.1	39.85	0.2	25.24	0.23	0.020	1.2	159
J0926+4504	-15.44	-14.22	-16.51	7.2	2.8	39.91	0.2	25.41	0.23	0.020	1.2	159
J1032+4919	-17.63	-16.21	-17.82	6.8	2.7	40.95	2.4	25.32	0.28	0.040	9.7	478
J1205+4551	-17.67	-16.32	-17.63	6.9	2.4	41.08	2.7	25.69	0.30	0.060	9.6	239
J1242+4851	-16.48	-15.88	-16.93	7.6	2.0	40.54	0.8	25.62
J1355+4651	-14.88	-14.93	-16.31	5.8	3.3	39.68	0.1	25.37	0.09	0.016	3.9	124

^a $M_{\text{FUV}}^{\text{SED}}$ is the absolute FUV magnitude derived from the intrinsic rest-frame SED.

^b M_{FUV} is the absolute FUV magnitude derived from the apparent *GALEX* magnitude.

^c M_g is the absolute SDSS *g* magnitude corrected for the Milky Way extinction.

^d M_\star is the total stellar mass (young + older population) in solar masses.

^eStarburst age in Myr.

^f $L(\text{H}\beta)$ is the extinction-corrected *H* β luminosity in erg s^{-1} .

^gSFR is the star-formation rate in $M_\odot \text{yr}^{-1}$.

^h ξ_{ion} is the ionizing photon production efficiency in Hz erg^{-1} defined as $\xi_{\text{ion}} = N_{\text{LyC}}/L_\nu$, where N_{LyC} is the Lyman continuum photon production rate derived from the extinction-corrected *H* β luminosity and L_ν is the monochromatic luminosity at $\lambda = 1500\text{\AA}$ derived from the intrinsic rest-frame SED.

ⁱ α is the exponential disc scale length in kpc.

^j r_{50} is the galaxy radius in kpc where the NUV intensity is equal to half of the maximal intensity.

^k Σ_1 is the star-formation rate surface density in $M_\odot \text{yr}^{-1} \text{kpc}^{-2}$, assuming the galaxy radius to be equal to α .

^l Σ_2 is the star-formation rate surface density in $M_\odot \text{yr}^{-1} \text{kpc}^{-2}$, assuming the galaxy radius to be equal to r_{50} .

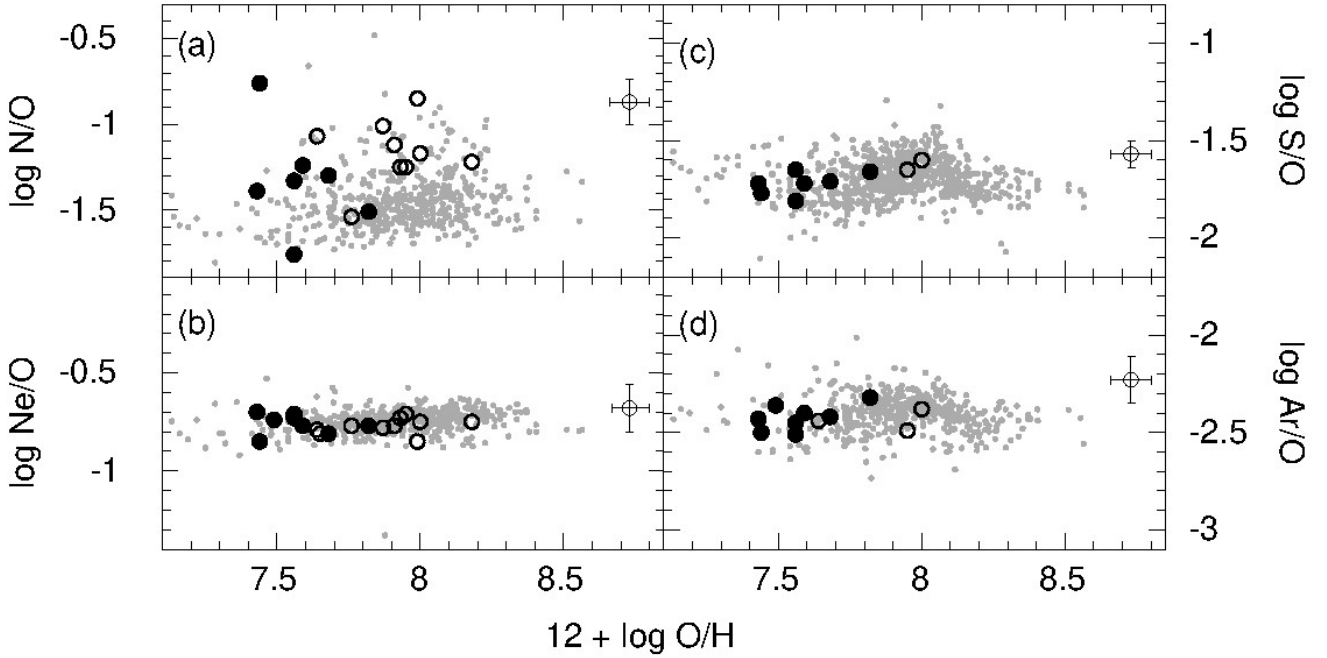


Figure 3. Dependences of heavy element-to-oxygen abundance ratios on oxygen abundance. In all panels, galaxies from this paper and LyC leaking galaxies (Izotov et al. 2016a,b, 2018a,b) are shown by filled circles and open circles, respectively. The compact SFGs from the SDSS (Izotov et al. 2016c) are represented by grey dots. Solar values by Lodders (2003) are shown by open circles with error bars.

2002). On the other hand, the corresponding surface densities of SFR in the studied galaxies $\Sigma = \text{SFR}/(\pi\alpha^2)$ are comparable to those of LyC leakers. Because of the compactness of the bright star-forming regions, the half-light radii r_{50} of our galaxies in the NUV are considerably smaller than α (see Table 3). Adopting r_{50} as a measure of the size of these galaxies (Table 3), the corresponding Σ s are typically two or-

ders of magnitude larger, and comparable to those found for low-redshift LyC leakers and SFGs at high redshifts (Curtis-Lake et al. 2016; Paulino-Afonso et al. 2018; Bouwens et al. 2017a).

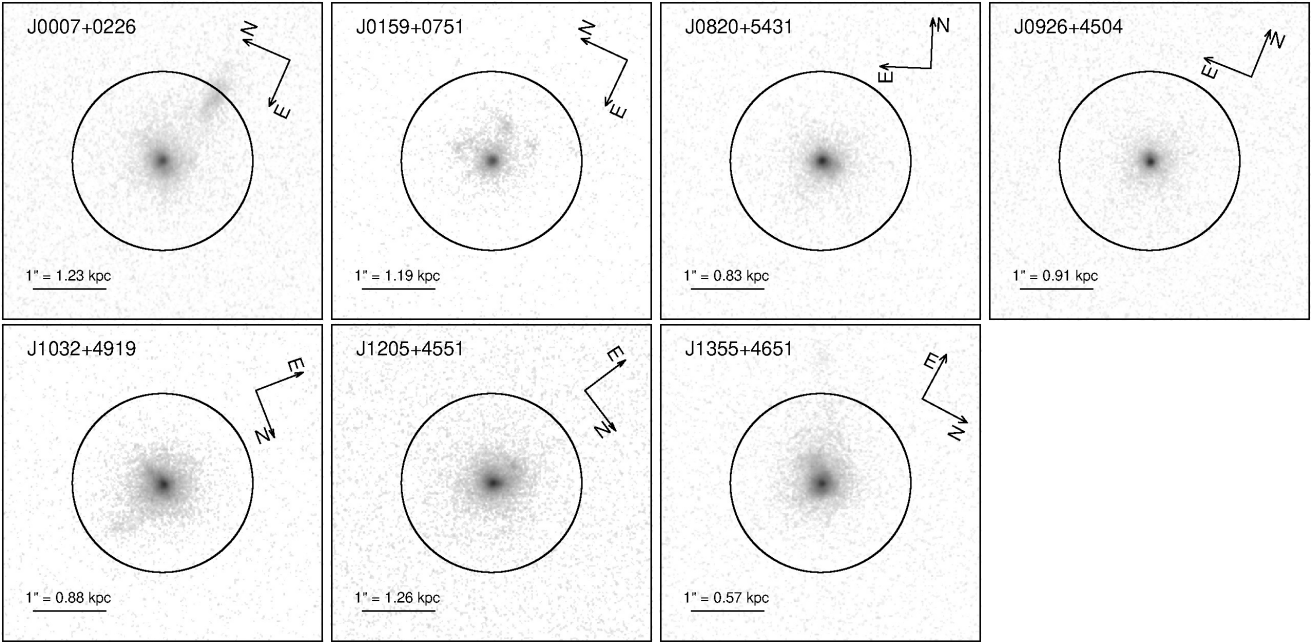


Figure 4. The *HST* NUV acquisition images of selected galaxies in log surface brightness scale. The image for J1242+4851 is not shown (see text). The COS spectroscopic aperture with a diameter of 2.5 arcsec is shown in all panels by a circle. The linear scale in each panel is derived adopting the angular size distance (Table 1).

Table 4. *HST*/COS observations

Name	Date	Exposure time (s)	
		MIRRORA	G130M
J0007+0226	2018-10-30	2×1398	5616
J0159+0751	2018-01-26	2×500	4245
J0820+5431	2019-02-25	2×1494	6001
J0926+4504	2019-02-22	2×1470	5905
J1032+4919	2018-11-18	2×440	4645
J1205+4551	2019-01-03	2×610	7470
J1242+4851	2018-12-22	2×0	6890
J1355+4651	2019-02-22	2×670	7350

5 LY α EMISSION

The LyC emission can not be directly observed in our galaxies because of their low redshifts. Therefore, we wish to use the Ly α profiles in their spectra to derive information about possible leaking LyC radiation for galaxies with much lower stellar masses than those of confirmed LyC leakers. [Dijkstra et al. \(2016\)](#) and [Verhamme et al. \(2017\)](#) have proposed that the presence of a double-peaked Ly α profile, with a small peak separation, would be a good indicator of LyC leakage. According to the models of [Verhamme et al. \(2015\)](#), the peak separation decreases with decreasing column density of the neutral gas. This in turn would result in a higher escape fraction of the LyC radiation. Additionally, the role of the blue Ly α peak in the LyC escape has been discussed by e.g. [Henry et al. \(2015\)](#) and [Orlitová et al. \(2018\)](#). They found that the escape fraction of the Ly α radiation increases when the blue peak velocity decreases.

The Ly α profiles in the medium-resolution spectra of the 8 observed galaxies are shown in Fig. 6. In the upper panel for each object, both the flux and the wavelength are

scaled so that the continuum behaviour can be seen over a broader wavelength range around the Ly α line, while in the lower panel both the flux and the wavelength scales are adjusted to examine the profile of the Ly α emission line. A strong Ly α $\lambda 1216 \text{ \AA}$ emission-line without any evidence for an absorption profile is detected in five galaxies (Fig. 6b,c,f,g,h), similarly to the low- z LyC leakers (fig. 7 in [Verhamme et al. 2017](#)). In the remaining 3 galaxies, the weak Ly α emission line is superposed on a broad absorption component (Fig. 6a,d,e). The fraction of galaxies with a detected Ly α absorption line is similar to that obtained by [McKinney et al. \(2019\)](#). However, the intensity at the bottom of the absorption lines is above zero in these galaxies, indicating that the covering factor of the H I cloud surrounding the ionizing source is less than unity, allowing for some Ly α emission and some continuum emission in this wavelength range to escape. The full widths at zero intensity of the Ly α emission lines in all our galaxies are $\text{FWZI} = 3 - 4 \text{ \AA}$ (Fig. 6). On the other hand, the widths of the absorption lines at the bottom of their profiles are considerably broader, $\sim 10 - 20 \text{ \AA}$ in the three galaxies J0007+0226, J0926+4504 and J1032+4919. Therefore, it is unlikely that the emission above zero at the bottom of the absorption profiles is due to the Ly α emission line.

Six out of eight observed galaxies show double-peaked Ly α emission profiles with the peak separations much larger than the nominal COS spectral resolution of $\sim 20 \text{ km s}^{-1}$ for the G130M grating. The Ly α emission line in J0926+4504 is too weak to definitely derive its profile. The two-peak shape is similar to that observed in known LyC leakers ([Izotov et al. 2016a,b](#), [2018a,b](#); [Verhamme et al. 2017](#)) and in GP galaxies ([Jaskot & Oey 2014](#); [Henry et al. 2015](#); [Yang et al. 2017a](#); [McKinney et al. 2019](#)). The Ly α emission-line profile of J1032+4919 is more complex and consists of three peaks, similar to that of one low- z LyC leaker ([Izotov et al. 2018b](#)),

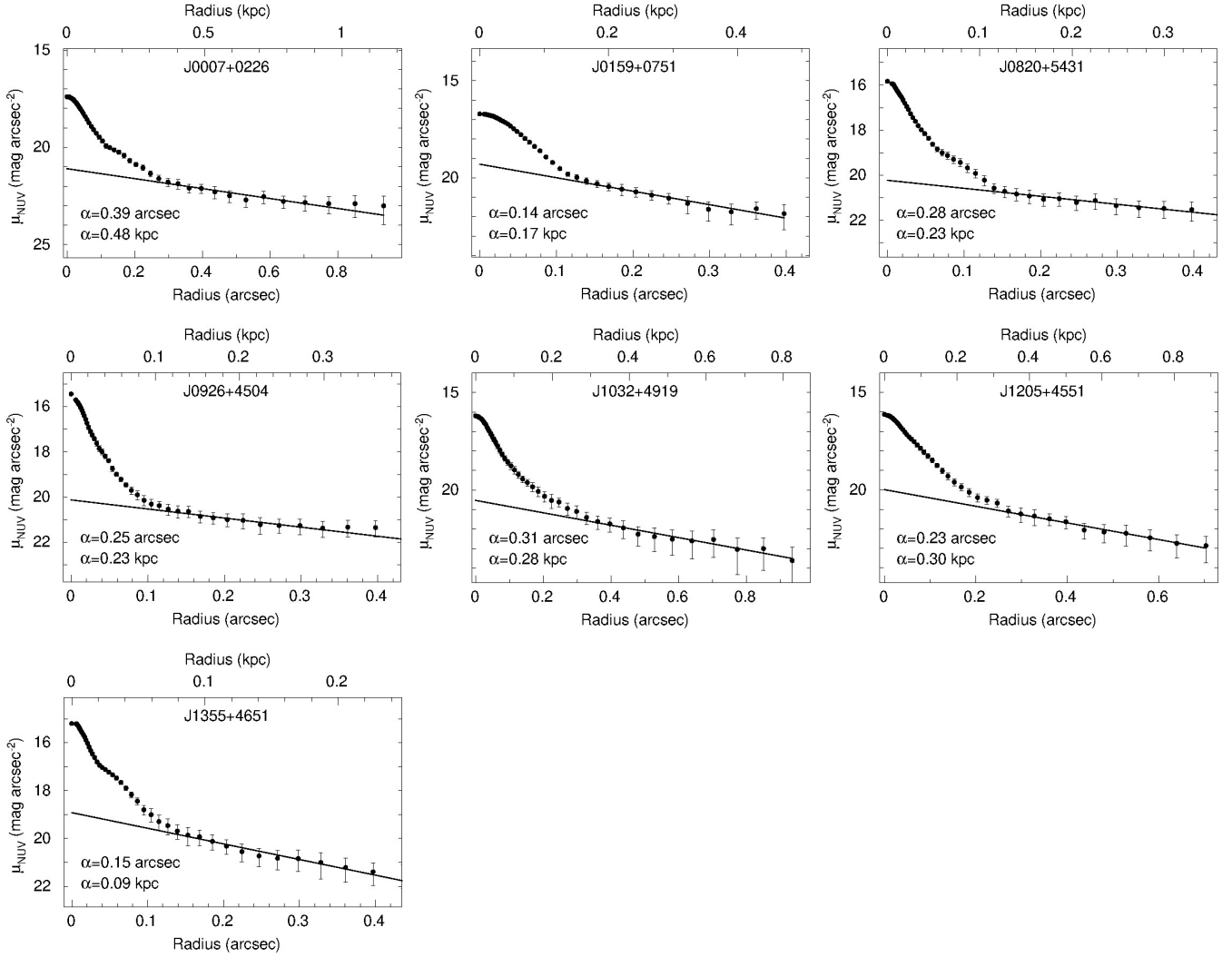


Figure 5. NUV surface brightness profiles of galaxies with the highest O_{32} ratio. The profile for J1242+4851 is not shown. The linear fits to the surface brightness profiles of the outer galaxy parts are shown by solid lines.

and two $z > 2$ LyC leakers (Vanzella et al. 2018; Rivera-Thorsen et al. 2017). However, at variance with J1032+4919, all other triple-peaked spectra in the literature do not show clear signs of underlying Ly α absorption.

Some parameters of the Ly α emission profile are presented in Table 5. The Ly α emission-line fluxes in the spectra of galaxies with detected broad Ly α absorption are measured placing the continuum at the bottom of the absorption profiles. For J1032+4919, two separations (blue peak - centre peak and centre peak - red peak) are given. It is seen that the separation between the peaks is in a narrow range $\sim 240 - 310 \text{ km s}^{-1}$, indicating low neutral hydrogen column densities $N(\text{H I})$ and implying considerable fractions of escaping LyC emission. However, in the spectra of three galaxies, J0007+0226, J0926+4504 and J1032+4919, strong Ly α absorption is present as well. The flux in the central part of absorption profiles is above zero, although their shape indicates that they are clearly saturated. This appearance is in contrast to expectations for a single source surrounded by an uniform neutral gas cloud with high $N(\text{H I})$. We derive

$N(\text{H I})$ using the relation

$$I(\lambda) = I_{\text{cont}} \exp[-\tau(\lambda)], \quad (1)$$

where I_{cont} and $I(\lambda)$ are the flux of the continuum and the flux in the line at the wavelength λ , respectively, after subtraction of the flux at the bottom of the Ly α absorption line. The optical depth $\tau(\lambda)$ in the Ly α profile at the wavelength λ is defined by the relation of Bohlin (1975)

$$\tau(\lambda) = 4.26 \times 10^{-20} \frac{N(\text{H I})}{6.04 \times 10^{-10} + (\lambda - \lambda_0)^2}, \quad (2)$$

where $N(\text{H I})$ is in cm^{-2} , λ is in \AA , $\lambda_0 = 1215.67 \text{ \AA}$. Using Eqs. 1 and 2 we find $N(\text{H I}) = 1.8 \times 10^{21} \text{ cm}^{-2}$, $1.0 \times 10^{21} \text{ cm}^{-2}$ and $3.0 \times 10^{21} \text{ cm}^{-2}$ from the fit of wings of absorption Ly α profiles in the spectra of J0007+0226, J0926+4504 and J1032+4919, respectively (grey lines in the upper panels of Fig. 6a, 6d, and 6e). We note that only the blue damped wing was used for fitting because the red wing is contaminated by the stellar $\text{N v } \lambda 1240 \text{ \AA}$ line with a P Cygni profile. Then the superposition of the Ly α absorption and emission lines could be explained by the emission of two star-forming

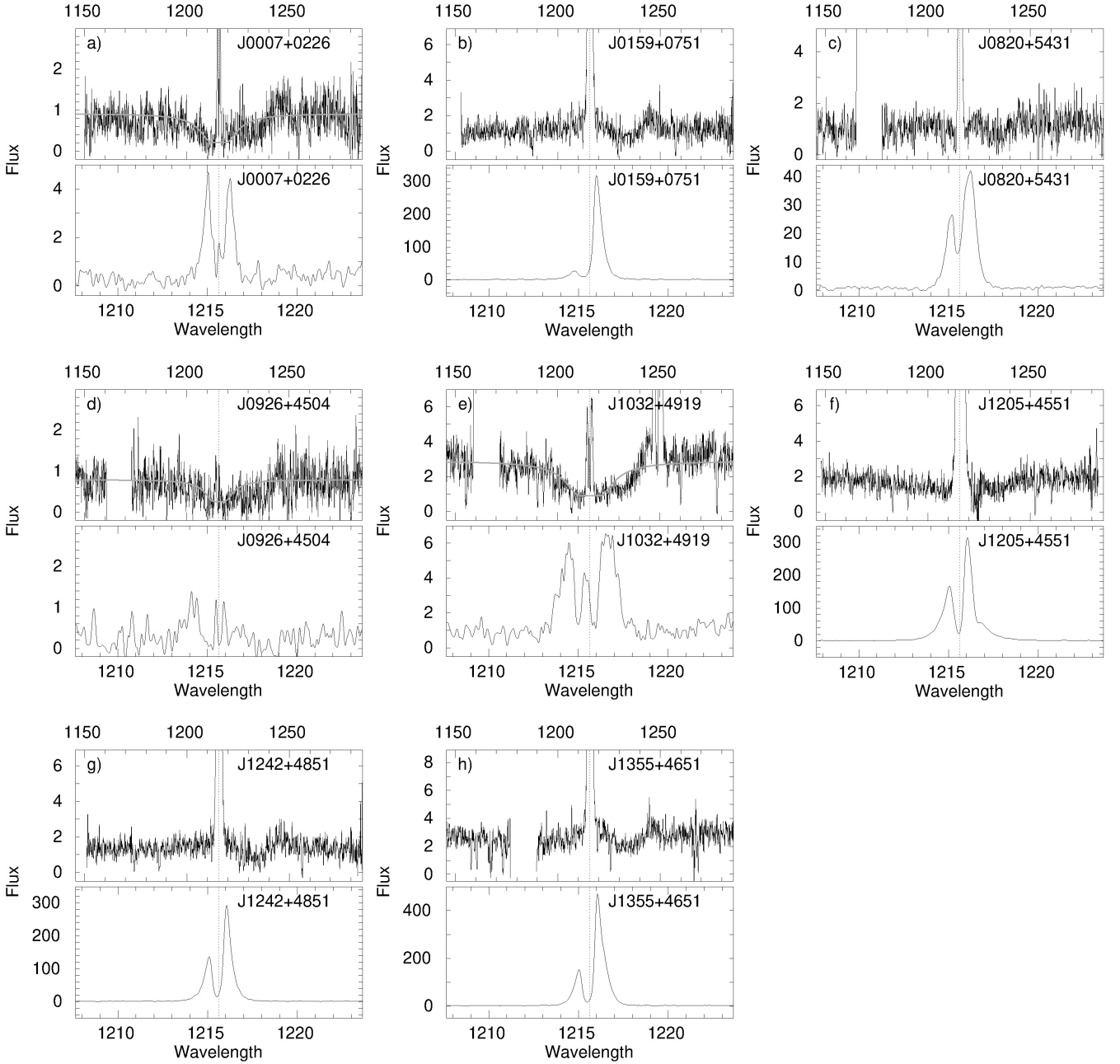


Figure 6. $Ly\alpha$ profiles. Vertical dotted lines indicate the centres of profiles. Upper panels for each object, with the rest-frame wavelength scale on top, are adjusted so that the continuum can be seen in a wide range of wavelengths. Lower panels, with the rest-frame wavelength scale at bottom, are adjusted to see $Ly\alpha$ emission-line profile. The geocoronal $O\text{ I } \lambda 1301, 1304\text{\AA}$ emission in spectra was removed by considering only orbital night data in the affected wavelength range. This wavelength range has a shorter exposure time and a lower S/N. In particular, the depression and higher noise in the upper panel of f) for J1205+4551, at $\sim 1225\text{\AA}$, is caused by replacement of the total spectrum by the orbital night spectrum in the affected region. $O\text{ I } \lambda 1301, 1304\text{\AA}$ emission could not be removed for J1032+4919. Flux densities are in $10^{-16} \text{ erg s}^{-1} \text{ cm}^{-2} \text{\AA}^{-1}$ and wavelengths are in \AA .

regions, where the fainter one, with a flux in the continuum corresponding to the one at the bottom of the absorption profile, is surrounded by neutral gas with low $N(\text{H I})$, and the brighter one is surrounded by a neutral optically thick cloud. The flux of the continuum for the brighter region is determined by the difference between the observed flux outside the absorption profile and the flux at its bottom. The presence of $Ly\alpha$ emission in galaxies with broad $Ly\alpha$ absorp-

tion could also be explained by low-column-density holes in a thick cloud of neutral hydrogen.

Table 5. Parameters for the Ly α and H β emission lines

Name	$A(\text{Ly}\alpha)_{\text{MW}}^{\text{a}}$	$I(\text{Ly}\alpha)^{\text{b}}$	$\log L(\text{Ly}\alpha)^{\text{c}}$	$\text{EW}(\text{Ly}\alpha)^{\text{d}}$	$V_{\text{sep}}^{\text{e}}$	$I(\text{H}\beta)^{\text{f}}$	$f_{\text{esc}}(\text{Ly}\alpha)^{\text{g}}$	$f_{\text{esc}}(\text{LyC})^{\text{h}}$
J0007+0226	0.161	6.5 \pm 3.2	39.81	7.4 \pm 3.9	310.3 \pm 22.5	52.3 \pm 7.0	0.53 \pm 0.27	...
J0159+0751	0.767	452.1 \pm 6.7	41.61	160.2 \pm 2.4	311.5 \pm 4.0	99.3 \pm 13.0	19.54 \pm 2.57	9.08 \pm 3.00
J0820+5431	0.438	57.5 \pm 2.5	40.30	47.8 \pm 2.2	255.7 \pm 3.7	20.2 \pm 2.7	12.22 \pm 1.72	17.84 \pm 3.01
J0926+4504	0.173	2.0 \pm 1.9	38.93	2.2 \pm 2.1	...	34.4 \pm 4.5	0.25 \pm 0.24	...
J1032+4919	0.070	14.9 \pm 2.0	39.84	5.2 \pm 0.8	247.7 \pm 9.9	109.6 \pm 14.2	0.59 \pm 0.11	...
					281.3 \pm 9.9			
J1205+4551	0.138	435.1 \pm 4.9	41.66	189.5 \pm 3.2	248.8 \pm 3.2	115.0 \pm 15.0	16.24 \pm 2.12	19.48 \pm 3.01
J1242+4851	0.106	293.9 \pm 3.9	41.44	191.3 \pm 2.5	239.4 \pm 4.9	40.1 \pm 5.5	31.46 \pm 4.34	22.00 \pm 3.03
J1355+4651	0.156	461.9 \pm 2.9	40.93	175.7 \pm 1.2	259.9 \pm 4.5	51.2 \pm 6.7	38.72 \pm 5.07	16.92 \pm 3.01

^a $A(\text{Ly}\alpha)_{\text{MW}}$ is the Milky Way extinction at the observed wavelength of the Ly α emission line in mags, adopting Cardelli et al. (1989) reddening law with $R(V)=3.1$.

^b $I(\text{Ly}\alpha)$ is the Ly α flux density in 10^{-16} erg s^{-1} cm^{-2} measured in the COS spectrum and corrected for the Milky Way extinction.

^c $L(\text{Ly}\alpha)$ is the Ly α luminosity in erg s^{-1} corrected for the Milky Way extinction.

^d $\text{EW}(\text{Ly}\alpha)$ is the rest-frame equivalent width in \AA of the Ly α emission line. Rest-frame equivalent widths of Ly α absorption lines in J0007+0226, J0926+4504, and J1032+4919 are -15.7 ± 5.1 \AA , -20.6 ± 7.3 \AA , and -21.4 ± 3.1 \AA , respectively.

^e V_{sep} is the Ly α velocity peak separation in km s^{-1} .

^f $I(\text{H}\beta)$ is the extinction-corrected H β flux density in 10^{-16} erg s^{-1} cm^{-2} measured in the SDSS spectrum.

^g $f_{\text{esc}}(\text{Ly}\alpha)$ is the ratio in percentage of $I(\text{Ly}\alpha)/I(\text{H}\beta)$ to its case B value of 23.3.

^h $f_{\text{esc}}(\text{LyC})$ is the indirectly derived LyC escape fraction in percentage, using the value of V_{sep} and equation 2 in Izotov et al. (2018b).

6 DISCUSSION

6.1 Comparison with other galaxy samples

We compare our galaxies with those studied in other recent papers. All galaxies from the sample in this paper are dwarf systems with SDSS g absolute magnitudes $M_g \sim -16$ to -18 mag. Their absolute FUV magnitudes M_{FUV} , in the range -14 to -16 , compare well with the average $M_{\text{FUV}} \sim -15$ mag of the faintest spectroscopically confirmed LAEs at redshifts 2.9 - 6.7, similar to those of the sources believed to reionize the Universe (Maseda et al. 2018). Our galaxies are much more compact in the NUV continuum (Fig. 5) and have lower metallicities (Table 1) than most Ly α emitters (LAEs) and LyC leakers. They have high ionizing photon production efficiencies ξ_{ion} (Table 3), above the canonical value in log scale of $\log \xi_{\text{ion}} \sim 25.2$ in units of $\log \text{Hz erg}^{-1}$ adopted in high- z studies (e.g. Robertson et al. 2013) and similar to the values in LAEs at $z \sim 3 - 7$ (Harikane et al. 2018; Nakajima et al. 2018). These high values are a natural consequence of a very young starburst age (Table 3). High ξ_{ion} in our galaxies are also similar to those in confirmed low- z LyC leakers (e.g. Schaerer et al. 2016). If applicable to all high- z galaxies, such ξ_{ion} values would suffice to reionize the Universe with a constant escape fraction $f_{\text{esc}}(\text{LyC}) \sim 10$ per cent (e.g. Ouchi et al. 2009; Robertson et al. 2013; Dressler et al. 2015; Robertson et al. 2015; Khaire et al. 2016). However, we note that the ξ_{ion} values in Table 3 should be considered only as lower limits, as including possible escaping LyC radiation, which is not taken into account, would somewhat increase these values.

The high- z LAEs show a tight relation between the Ly α luminosity $L(\text{Ly}\alpha)$ and the absolute magnitude M_{FUV} at $\lambda = 1500\text{\AA}$ (small open grey circles in Fig. 7a). The confirmed LyC leakers (open black circles, Izotov et al. 2016a,b, 2018a,b) follow the same relation. On the other hand, GPs at redshifts $\lesssim 0.3$ (grey asterisks) are offset to lower $L(\text{Ly}\alpha)$ by one order of magnitude. This offset can be caused by aperture effects because GPs are on average closer to us and

have larger angular sizes. Furthermore, the $\text{EW}(\text{Ly}\alpha)$ s in GPs are considerably lower than in low- z LyC leakers (Fig. 7a), indicating older burst ages and thus lower Ly α luminosities. We note that for the LyC leakers and GPs we do not use the published values for Ly α in Izotov et al. (2016a,b, 2018a,b), Jaskot & Oey (2014), Henry et al. (2015), Jaskot et al. (2017) and Yang et al. (2017a). Instead for the sake of data homogeneity, we measured Ly α fluxes and equivalent widths using the public *HST* data, correcting the fluxes for Milky Way extinction and converting them to luminosities. As for the absolute FUV magnitudes, we derived them from the apparent GALEX FUV magnitudes.

Our galaxies with extreme O₃₂ extend the range of M_{FUV} to appreciably lower FUV brightnesses. Their low Ly α luminosities ($L(\text{Ly}\alpha) \lesssim 10^{42}$ erg s^{-1}) make the $L(\text{Ly}\alpha)$ - M_{FUV} relation bend downwards at low M_{FUV} (Fig. 7a)). We note that LAEs with low Ly α luminosities, similar to those of our galaxies, are also detected in the high- z Universe (e.g. de La Vieuville et al. 2019). A notable feature of the four galaxies with the highest $\text{EW}(\text{Ly}\alpha)$ and highest $L(\text{Ly}\alpha)$ in our sample is that their Ly α luminosities are lower by a factor > 2 than the value derived from the extrapolation of the relation for high- z galaxies to fainter absolute FUV magnitudes (dashed line). While they are consistent with the extrapolation of the trend defined by the GPs to fainter absolute UV magnitudes, the Ly α equivalent widths of the galaxies with extreme O₃₂ are similar to those of the low- z LyC leakers (Izotov et al. 2016a,b, 2018a,b) and are much higher than those of GPs.

It was shown e.g. by Wisotzki et al. (2016, 2018) that high- z galaxies at $z > 3$ are surrounded by extended diffuse Ly α -emitting haloes tracing neutral gas up to several tens of kpc and contributing 40 - 90 per cent of the total Ly α flux. These extended haloes are seen even in low-mass SFGs with stellar masses down to $10^8 - 10^9 M_{\odot}$ (Erb, Steidel & Chen 2018; Erb et al. 2019). Yang et al. (2017b) have shown that Ly α emission in Ly α -emitting galaxies at lower redshifts $z \lesssim 0.3$ is spatially more extended compared to that of the UV continuum.

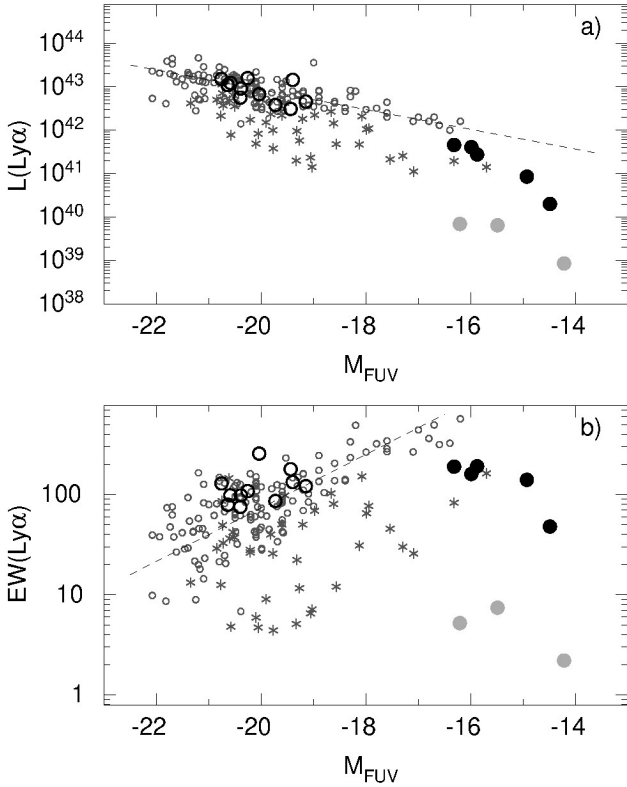


Figure 7. Dependence of absolute magnitude M_{FUV} at 1500\AA on **a)** $\text{Ly}\alpha$ luminosity $L(\text{Ly}\alpha)$ in erg s^{-1} and **b)** equivalent width $\text{EW}(\text{Ly}\alpha)$ in \AA . Galaxies from this paper with and without broad $\text{Ly}\alpha$ absorption profiles are shown by grey filled circles and black filled circles, respectively. The confirmed LyC leakers from Izotov et al. (2016a,b, 2018a,b) are shown by black open circles and GPs from *HST* programs GO 12928 (Henry et al. 2015), GO 13293 (Jaskot & Oey 2014), GO 14080 (Jaskot et al. 2017; McKinney et al. 2019), and GO 14201 (Yang et al. 2017a) are shown by grey asterisks. High-redshift galaxies from Ouchi et al. (2008), Hashimoto et al. (2017) and Jiang et al. (2013) are represented by small grey open circles. Relations obtained in this paper for high-redshift galaxies are shown by dashed lines in both panels.

The difference between our high- $\text{EW}(\text{Ly}\alpha)$ and high- z galaxies may possibly be caused by a low-intensity diffuse $\text{Ly}\alpha$ emission in our galaxies extending outside the extraction aperture used to obtain the one-dimensional spectrum. In this case, an aperture correction is needed for comparison of the $\text{Ly}\alpha$ flux with fluxes of other hydrogen emission lines. However, we do not expect a large aperture correction for $L(\text{Ly}\alpha)$ (> 2) because the adopted aperture for the extraction of one-dimensional spectra includes nearly all light from our galaxies. Additionally, we have compared $\text{Ly}\alpha$ fluxes in one-dimensional spectra obtained with different extraction apertures and reduced with the same custom and pipeline data reduction packages. We find that they differ by not more than 5 per cent. $\text{Ly}\alpha$ imaging of the lowest-mass SFGs, with stellar masses $\lesssim 10^8 M_{\odot}$, is needed to verify the importance of aperture corrections.

Other factors may play a role in reducing $L(\text{Ly}\alpha)$ in our low-mass galaxies, e.g. unaccounted contribution of underlying $\text{Ly}\alpha$ absorption, enhanced UV extinction due to a larger fraction of dust and/or a steeper reddening law in the UV

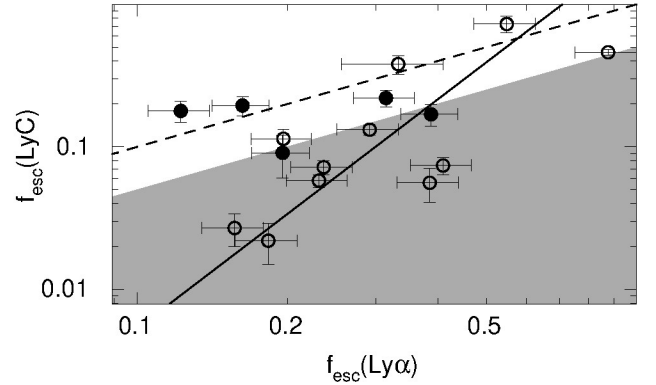


Figure 8. Relation between the $\text{Ly}\alpha$ escape fraction $f_{\text{esc}}(\text{Ly}\alpha)$ and the directly derived LyC escape fraction $f_{\text{esc}}(\text{LyC})$ for LyC leakers from Izotov et al. (2016a,b, 2018a,b) (open circles with 1σ error bars). The maximum likelihood fit to these data is shown by the solid line. The dashed line shows the relation $f_{\text{esc}}(\text{Ly}\alpha) = f_{\text{esc}}(\text{LyC})$. The five galaxies without $\text{Ly}\alpha$ absorption from this paper are represented by the filled circles. The LyC escape fractions for these galaxies $f_{\text{esc}}(\text{LyC})$ are indirectly derived from the peak velocity separations of $\text{Ly}\alpha$ profiles (Table 5). The shaded area shows the region occupied by the dusty clumpy models of Dijkstra et al. (2016).

range than in LyC leakers and high- z galaxies. But these factors are unlikely to be enough to explain the observed large offset of our galaxies from the extrapolated value (dashed line in Fig. 7a). We note that the $\text{H}\beta$ luminosities in our galaxies are more than one order of magnitude smaller than in the LyC leakers, corresponding to a smaller number of massive stars by the same factor. Probably, dynamical processes such as large-scale outflows due to the evolution of massive stars in our galaxies are considerably less energetic and may result in a reduced escaping $\text{Ly}\alpha$ emission.

The distribution of the $\text{Ly}\alpha$ rest-frame equivalent widths $\text{EW}(\text{Ly}\alpha)$ for the same samples of galaxies as in Fig. 7a is shown in Fig. 7b. The range of $\text{EW}(\text{Ly}\alpha)$ for our objects is larger than that for LyC leakers with four galaxies having $\text{EW}(\text{Ly}\alpha)$ smaller than those for LyC leakers, and four galaxies with $\text{EW}(\text{Ly}\alpha)$ greater than the average value for LyC leakers. On the other hand, GPs from the literature have in general considerably lower $\text{EW}(\text{Ly}\alpha)$. Comparing to high- z galaxies we note that the $\text{EW}(\text{Ly}\alpha)$ s of our galaxies are several times lower than of high- z galaxies, due to the same reasons (i.e possible aperture effects) as for $\text{Ly}\alpha$ luminosities.

Hashimoto et al. (2017) found a trend of increasing $\text{EW}(\text{Ly}\alpha)$ with decreasing UV luminosity. They attributed this trend to the lower metallicities of lower-luminosity galaxies. However, the distribution of our galaxies which extend the $\text{EW}(\text{Ly}\alpha)$ - M_{FUV} relation to lower UV luminosities does not support the existence of this trend. Although a dependence of $\text{EW}(\text{Ly}\alpha)$ on metallicity is not excluded, the relation in Fig. 7b can also be explained by increasingly higher $\text{EW}(\text{Ly}\alpha)$ errors at their high values for high- z galaxies and by the fact that only galaxies with high $\text{EW}(\text{Ly}\alpha)$ at high redshifts can be selected. The presence of many low- z GPs with low $\text{EW}(\text{Ly}\alpha)$ favours this selection effect.

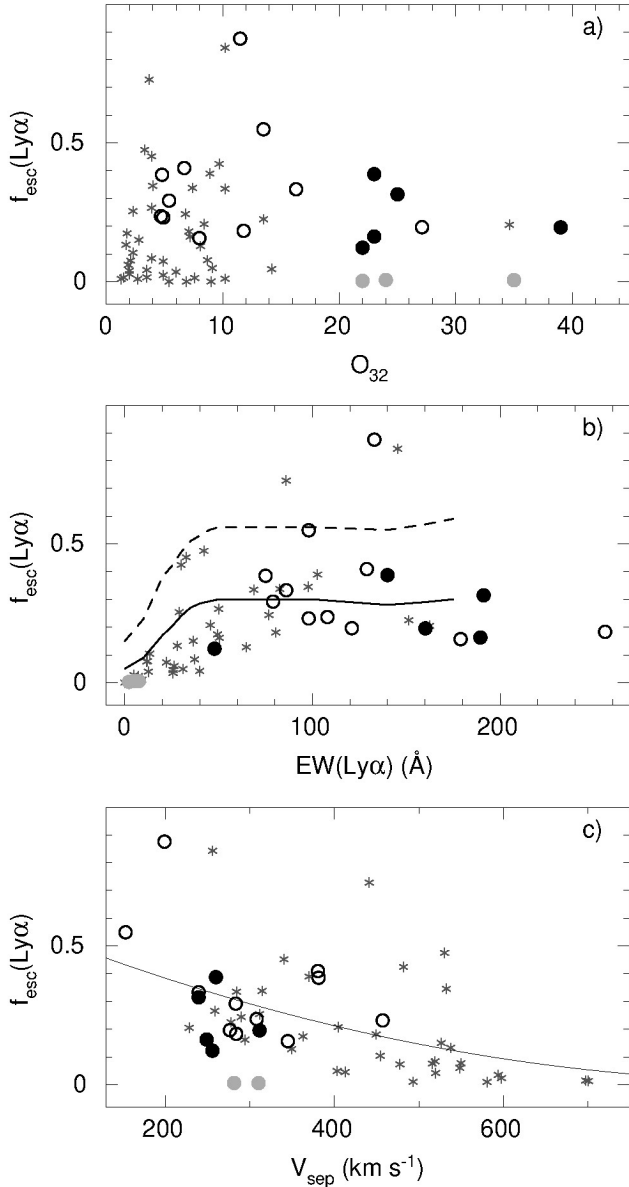


Figure 9. Dependence of the Ly α escape fraction $f_{\text{esc}}(\text{Ly}\alpha)$ on **a)** the $[\text{O III}]\lambda 5007/[\text{O II}]\lambda 3727$ flux ratio O_{32} , **b)** the rest-frame Ly α equivalent width $\text{EW}(\text{Ly}\alpha)$, and **c)** the separation between Ly α emission-line velocity peaks V_{sep} . Symbols are the same as in Fig. 7. Solid and dashed lines in **b)** are modelled relations by Sobral & Matthee (2019) for a fixed $E(B - V) = 0.2$ and 0.1 , respectively. The solid line in **c)** is the maximum likelihood fit to all data (Eq. 5).

6.2 The Ly α escape fraction

An important quantity to consider is the escape fraction $f_{\text{esc}}(\text{Ly}\alpha)$. In this paper we define $f_{\text{esc}}(\text{Ly}\alpha)$ as the ratio of the extinction-corrected Ly α to H β flux ratio to its Case B value of 23.3, corresponding to that at a low electron number density, $N_e \sim 10^2 \text{ cm}^{-3}$ (Storey & Hummer 1995):

$$f_{\text{esc}}(\text{Ly}\alpha) = \frac{1}{23.3} \frac{I(\text{Ly}\alpha)}{I(\text{H}\beta)}, \quad (3)$$

where $I(\text{Ly}\alpha)$ is the flux density corrected for the Milky Way extinction, and $I(\text{H}\beta)$ is the flux density corrected for both

the Milky Way and internal galaxy extinction. At higher electron densities, for example at $N_e \sim 10^3 \text{ cm}^{-3}$, the Case B Ly $\alpha/\text{H}\beta$ ratio is higher by ~ 10 per cent, resulting in a lower $f_{\text{esc}}(\text{Ly}\alpha)$. Using Eq. 3, we calculate $f_{\text{esc}}(\text{Ly}\alpha)$ for the eleven LyC leakers from Izotov et al. (2016a,b, 2018a,b) and compare them with their directly measured $f_{\text{esc}}(\text{LyC})$ in Fig. 8. It is seen that there is a general trend of increasing $f_{\text{esc}}(\text{LyC})$ with increasing $f_{\text{esc}}(\text{Ly}\alpha)$. That trend can be approximated by the maximum likelihood relation (solid line)

$$\log f_{\text{esc}}(\text{LyC}) = (2.67 \pm 0.51) \times \log f_{\text{esc}}(\text{Ly}\alpha) + (0.40 \pm 0.29), \quad (4)$$

but with large uncertainties. The distribution of the data points in Fig. 8 is somewhat different from that of the dusty, clumpy interstellar medium models of Dijkstra et al. (2016) (shaded region in Fig. 8). Their models predict $f_{\text{esc}}(\text{Ly}\alpha) \gtrsim 2 \times f_{\text{esc}}(\text{LyC})$ and a wide range of $f_{\text{esc}}(\text{Ly}\alpha)$ at fixed $f_{\text{esc}}(\text{LyC})$, depending on the covering factor of the neutral gas. The observational data show a much narrower range of $f_{\text{esc}}(\text{Ly}\alpha)$ at fixed $f_{\text{esc}}(\text{LyC})$, with some galaxies lying outside the model prediction regions. A relatively small dispersion of the data points in the observed relation in Fig. 8 gives hope that $f_{\text{esc}}(\text{Ly}\alpha)$ can be used to indirectly derive $f_{\text{esc}}(\text{LyC})$. However, the number of confirmed LyC leakers is still very small and larger statistics are needed to verify the relation given by Eq. 4. There is also the possibility that there exist sources with significant Ly α escape but with no leaking LyC radiation which would flatten the relation shown by the solid line.

The filled circles in Fig. 8 show the galaxies from our sample with the exclusion of the three galaxies with Ly α absorption. For these galaxies, $f_{\text{esc}}(\text{LyC})$ is derived using the velocity separation between the peaks of Ly α emission lines. It is seen that, for a given $f_{\text{esc}}(\text{LyC})$, the galaxies are offset from the confirmed LyC leakers to lower $f_{\text{esc}}(\text{Ly}\alpha)$. Possible aperture corrections for Ly α emission would be too small to account for those offsets. On the other hand, corrections for unaccounted Ly α absorption would increase $f_{\text{esc}}(\text{Ly}\alpha)$. Overall, these corrections do not appear to be enough to account for the offsets. Alternatively, parts of the offsets could be due to an overestimation of the indirect value of $f_{\text{esc}}(\text{LyC})$, as determined by eq. 2 of Izotov et al. (2018b).

It was suggested by Nakajima & Ouchi (2014) that the fraction of escaping ionizing radiation from galaxies correlates with the O_{32} ratio. However, Izotov et al. (2018b) found that the $\text{O}_{32} - f_{\text{esc}}(\text{LyC})$ correlation for the confirmed LyC leakers is rather weak and a high O_{32} does not guarantee a high $f_{\text{esc}}(\text{LyC})$. Adopting the correlation between the Ly α and LyC escape fractions (Fig. 8), we investigate whether O_{32} can be used as indirect indicator of escaping ionizing radiation for galaxies with the highest O_{32} . We show in Fig. 9a the $\text{O}_{32} - f_{\text{esc}}(\text{Ly}\alpha)$ diagram for the same galaxies as in Fig. 7, excluding the high- z LAEs. The galaxies discussed in this paper (filled circles) extend the range of O_{32} up to ~ 40 , a factor of two higher than in previous studies. However, no correlation is found. Thus, we confirm and strengthen the conclusion of Izotov et al. (2018b) that O_{32} is not a reliable indicator of escaping Ly α emission and likely also of escaping LyC radiation. This conclusion is in agreement with the models of Bassett et al. (2019) who have shown that galaxies with various metallicities and ionization parameters fill all the $f_{\text{esc}}(\text{LyC}) - \text{O}_{32}$ space. However, we note that $f_{\text{esc}}(\text{Ly}\alpha)$

for our galaxies (filled circles in Fig. 9) could be somewhat higher because of unaccounted possible aperture corrections for Ly α emission and underlying absorption.

We discuss other possible indicators of $f_{\text{esc}}(\text{Ly}\alpha)$. A possible candidate is the rest-frame equivalent width $\text{EW}(\text{Ly}\alpha)$. The diagram $\text{EW}(\text{Ly}\alpha) - f_{\text{esc}}(\text{Ly}\alpha)$ is shown in Fig. 9b. This diagram is somewhat puzzling. At low $\text{EW}(\text{Ly}\alpha)$, the Ly α escape fraction $f_{\text{esc}}(\text{Ly}\alpha)$ increases with increasing $\text{EW}(\text{Ly}\alpha)$. However, no such dependence is found at high $\text{EW}(\text{Ly}\alpha) \gtrsim 60\text{\AA}$ for four of our galaxies and three confirmed LyC leakers with the highest $\text{EW}(\text{Ly}\alpha)$. One possible explanation for that behavior has been proposed by Sobral & Matthee (2019). They have shown that the $\text{EW}(\text{Ly}\alpha) - f_{\text{esc}}(\text{Ly}\alpha)$ relation flattens considerably in the presence of dust absorption and is nearly independent of $\text{EW}(\text{Ly}\alpha)$, given a varying ionizing photon production efficiency ξ_{ion} . In particular, our data, in the flat part of the diagram at $\text{EW}(\text{Ly}\alpha) \gtrsim 150\text{\AA}$, can be reproduced adopting $E(B-V) \sim 0.2$ mag, corresponding to $C(\text{H}\beta) \sim 0.3$, given that $\log \xi_{\text{ion}}$ increases from ~ 25.0 to ~ 25.7 with increasing $\text{EW}(\text{Ly}\alpha)$ (solid line in Fig. 9b). This value of $C(\text{H}\beta)$ is somewhat higher than the values derived from the SDSS spectra (Table 5), but is consistent with the values obtained from the high signal-to-noise ratio LBT spectra for J0159+0751, J1032+4919, J1205+4551 and J1355+4651 (Izotov et al. 2017).

Another indirect indicator of escaping radiation is the velocity separation between Ly α peaks V_{sep} . Izotov et al. (2018b) have found a tight correlation between $f_{\text{esc}}(\text{LyC})$ and V_{sep} . Fig. 9c shows a possible correlation between the peak separation V_{sep} and the Ly α escape fraction $f_{\text{esc}}(\text{Ly}\alpha)$, described by the maximum likelihood relation (solid line in Fig. 9c):

$$f_{\text{esc}}(\text{Ly}\alpha) = 6.56 \times 10^{-7} V_{\text{sep}}^2 - 1.25 \times 10^{-3} V_{\text{sep}} + 0.607. \quad (5)$$

The large scatter of the data around the relation found between an integrated property of Ly α ($f_{\text{esc}}(\text{Ly}\alpha)$) and a characteristic of the Ly α profile (V_{sep}) is probably to be expected, since several physical properties, such as dust content, H I column density, H I kinematics and geometry affect the Ly α radiative transfer (see e.g. Schaerer et al. 2011; Verhamme et al. 2015).

Finally, we consider whether He I emission lines in the optical range can be indicators of Ly α emission. Izotov et al. (2017) have argued that He I emission line ratios are promising diagnostics because some of these lines can be optically thick, indicating a high column density of the neutral gas. The He I $\lambda 3889\text{\AA}$ emission line is most sensitive to this effect. This line is blended with the hydrogen H8 $\lambda 3889\text{\AA}$ emission line, and its intensity can be obtained by subtracting the H8 intensity equal to $0.107 \times I(\text{H}\beta)$.

The recombination intensity of the He I $\lambda 3889\text{\AA}$ emission line is $\sim 0.1 \times I(\text{H}\beta)$. This line can be enhanced by collisions with electrons but weakened if its optical depth is high. Therefore, the condition $I(\text{He I } \lambda 3889)/I(\text{H}\beta) < 0.1$, corresponding to $I(\text{H8} + \text{He I } \lambda 3889)/I(\text{H}\beta) < 0.2$, would be an indication of high optical depth and high $N(\text{H I})$.

It is seen in Table A1 that $I(\text{H8} + \text{He I } \lambda 3889)/I(\text{H}\beta)$ is considerably lower than 0.2 in only two galaxies, J0926+4504 and J1032+4919. Both of these show broad Ly α absorption line in their spectra (Fig. 6d,e), indicating high $N(\text{H I})$. For the remaining galaxies, this technique predicts lower $N(\text{H I})$ and thus stronger Ly α in emission. The technique fails for

only one galaxy, J0007+0226, which shows Ly α absorption in its spectrum (Fig. 6a), but has $I(\text{H8} + \text{He I } \lambda 3889)/I(\text{H}\beta) \sim 0.2$. Thus we conclude that the He I $\lambda 3889\text{\AA}$ emission line is generally a good indicator of $N(\text{H I})$, and hence of Ly α emission.

7 CONCLUSIONS

We present here new *HST*/COS observations of eight low-redshift ($z < 0.07$) compact star-forming galaxies (SFG) with extremely high O₃₂ in the range $\sim 22 - 39$. All studied objects are compact low-mass ($\log(M_{\star}/M_{\odot}) = 5.8 - 8.6$) and low-metallicity ($12 + \log(\text{O}/\text{H}) = 7.43 - 7.82$) galaxies with strong nebular emission lines in their spectra ($\text{EW}(\text{H}\beta) = 258 - 483\text{\AA}$), indicating very young starburst ages of $0.5 - 3.3$ Myr. The Ne/O, S/O and Ar/O abundance ratios in our galaxies are similar to the values for the bulk of compact SDSS SFGs. On the other hand, similarly to confirmed LyC leakers, the N/O abundance ratios in our galaxies are higher than those of the most compact SDSS SFGs. We also study the Ly α emission and indirect indicators of the escaping Ly α and Lyman continuum (LyC) radiation of these SFGs. Our main results are summarized as follows:

1. A strong Ly α emission line with two peaks was observed in the spectra of five galaxies, while a Ly α emission line with a low equivalent width on top of a broad Ly α absorption profile is present in the remaining three galaxies. Using the damped wings of these absorption profiles, we derive neutral hydrogen column densities $N(\text{H I})$ in the range $(1 - 3) \times 10^{21} \text{ cm}^{-2}$.

2. We discuss various indirect indicators of escaping Ly α and ionizing radiation, such as the O₃₂ ratio, $\text{EW}(\text{Ly}\alpha)$ and the velocity separation between Ly α emission line peaks V_{sep} , assuming that the strength of the Ly α emission line is a measure of LyC leakage. We found that there is no correlation between O₃₂ and the Ly α escape fraction $f_{\text{esc}}(\text{Ly}\alpha)$. The dependence of $f_{\text{esc}}(\text{Ly}\alpha)$ on $\text{EW}(\text{Ly}\alpha)$ is such that at low $\text{EW}(\text{Ly}\alpha) \lesssim 100\text{\AA}$, there is a linear increase of $f_{\text{esc}}(\text{Ly}\alpha)$, while at high $\text{EW}(\text{Ly}\alpha) > 150\text{\AA}$, $f_{\text{esc}}(\text{Ly}\alpha)$ is nearly constant with a value ~ 0.25 . This behavior may be explained by dust absorption. We find a trend of increasing of $f_{\text{esc}}(\text{Ly}\alpha)$ with decreasing of V_{sep} . However, even galaxies showing double-peaked Ly α profiles exhibit a large scatter between the Ly α escape fraction and the separation of their peaks V_{sep} . The latter quantity has been shown to correlate more strongly with the LyC escape fraction (Izotov et al. 2018b).

3. Bright compact star-forming regions are seen in the COS near ultraviolet (NUV) acquisition images. The surface brightness profile at the outskirts can be approximated by an exponential disc profile, with a scale length of $\sim 0.09 - 0.48$ kpc. These scale lengths are several times lower than those of confirmed LyC leakers and are among the lowest ones found for local blue compact dwarf galaxies.

The global properties of the selected galaxies are very similar to those of the lowest-mass high- z galaxies. They are thus ideal nearby laboratories for investigating the mechanisms responsible for the escape of Ly α and ionizing radiation from galaxies during the epoch of the reionization of the Universe.

ACKNOWLEDGEMENTS

We thank the anonymous referee for valuable comments. These results are based on observations made with the NASA/ESA *Hubble Space Telescope*, obtained from the data archive at the Space Telescope Science Institute. STScI is operated by the Association of Universities for Research in Astronomy, Inc. under NASA contract NAS 5-26555. Support for this work was provided by NASA through grant number HST-GO-15136.002-A from the Space Telescope Science Institute, which is operated by AURA, Inc., under NASA contract NAS 5-26555. Y.I.I. and N.G.G. acknowledge support from the National Academy of Sciences of Ukraine (Project No. 0116U003191) and by its Program of Fundamental Research of the Department of Physics and Astronomy (Project No. 0117U000240) of the National Academy of Sciences of Ukraine. G.W. has been supported by the Deutsches Zentrum für Luft- und Raumfahrt (DLR) through grant number 50OR1720. I.O. acknowledges grants GACR 14-20666P and 17-06217Y of the Czech National Foundation. Funding for the Sloan Digital Sky Survey IV has been provided by the Alfred P. Sloan Foundation, the U.S. Department of Energy Office of Science, and the Participating Institutions. SDSS-IV acknowledges support and resources from the Center for High-Performance Computing at the University of Utah. The SDSS web site is www.sdss.org. SDSS-IV is managed by the Astrophysical Research Consortium for the Participating Institutions of the SDSS Collaboration. GALEX is a NASA mission managed by the Jet Propulsion Laboratory. This publication makes use of data products from the Wide-field Infrared Survey Explorer, which is a joint project of the University of California, Los Angeles, and the Jet Propulsion Laboratory/California Institute of Technology, funded by the National Aeronautics and Space Administration. GALEX is a NASA mission managed by the Jet Propulsion Laboratory. This research has made use of the NASA/IPAC Extragalactic Database (NED) which is operated by the Jet Propulsion Laboratory, California Institute of Technology, under contract with the National Aeronautics and Space Administration.

REFERENCES

- Abolfathi B. et al., 2018, *ApJS*, 235, 42
Ade P. A. R. et al., 2014, *A&A*, 571, 16
Baldwin J. A., Phillips M. M., Terlevich R., 1981, *PASP*, 93, 5
Bassett et al., 2019, *MNRAS*, 493, 5223
Bian F., Fan X., McGreer I., Cai Z., Jiang L., 2017, *ApJ*, 837, 12
Bohlin R. C., 1975, *ApJ*, 200, 402
Borthakur S., Heckman T. M., Leitherer C., Overzier R. A., 2014, *Science*, 346, 216
Bouwens R. J., Illingworth G. D., Oesch P. A., Caruana J., Holwerda B., Smit R., Wilkins S., 2015, *ApJ*, 811, 140
Bouwens R. J., Illingworth G. D., Oesch P. A., Atek H., Lam D., Stefanon M., 2017a, *ApJ*, 843, 41
Bouwens R. J., Oesch P. A., Illingworth G. D., Ellis R. S., Stefanon M., 2017b, *ApJ*, 843, 129
Cardamone C. et al., 2009, *MNRAS*, 399, 1191
Cardelli J. A., Clayton G. C., Mathis J. S., 1989, *ApJ*, 345, 245
Chisholm J., Orlitová I., Schaerer D., Verhamme A., Worseck G., Izotov Y. I., Thuan T. X., Guseva N. G., 2017, *A&A*, 605, 67
Chisholm J. et al., 2018, *A&A*, 616, 30
Curtis-Lake E. et al., 2016, *MNRAS*, 457, 440
de Barros S. et al., 2016, *A&A*, 585, 51
Dijkstra M., Gronke M., Venkatesan A., 2016, *ApJ*, 828, 71
Dressler A., Henry A., Martin C. L., Sawicki M., McCarthy P., Villaneuva E., 2015, *ApJ*, 806, 19
Erb D. K., Steidel C. C., Chen Y., 2018, *ApJ*, 862, 10
Erb D. K., Berg D. A., Auger M. W., Kaplan D. L., Brammer G., Pettini M., 2019, *ApJ*, 884, 7
Faisst A. L., 2016, *ApJ*, 829, 99
Fletcher T. J., Tang M., Robertson B. E., Nakajima K., Ellis R. S., Stark D. P., Inoue A., 2019, *ApJ*, 878, 87
Grazian A. et al., 2016, *A&A*, 585, 48
Guseva N. G., Izotov Y. I., Fricke K. J., Henkel C., 2013, *A&A*, 555, 90
Harikane Y. et al., 2018, *ApJ*, 859, 84
Hashimoto T. et al., 2017, *A&A*, 608, 10
Hassan S., Davé R., Mitra S., Finlator K., Ciardi B., Santos M. G., 2018, *MNRAS*, 473, 227
Henry A., Scarlata C., Martin C. S., Erb D., 2015, *ApJ*, 809, 19
Hernandez S., Leitherer C., Boquien M., Buat V., Burgarella D., Calzetti D., Noll S., 2018, *MNRAS*, 478, 1292
Inoue A. K., Shimizu I., Iwata I., Tanaka M., 2014, *MNRAS*, 442, 1805
Izotov Y. I., Thuan T. X., Lipovetsky V. A., 1994, *ApJ*, 435, 647
Izotov Y. I., Stasińska G., Meynet G., Guseva N. G., Thuan T. X., 2006, *A&A*, 448, 955
Izotov Y. I., Guseva N. G., Thuan T. X., 2011, *ApJ*, 728, 161
Izotov Y. I., Orlitová I., Schaerer D., Thuan T. X., Verhamme A., Guseva N. G., Worseck G., 2016a, *Nature*, 529, 178
Izotov Y. I., Schaerer D., Thuan T. X., Worseck G., Guseva N. G., Orlitová I., Verhamme A., 2016b, *MNRAS*, 461, 3683
Izotov Y. I., Guseva N. G., Fricke K. J., Henkel C., 2016c, *MNRAS*, 462, 4427
Izotov Y. I., Thuan T. X., Guseva N. G., 2017, *MNRAS*, 471, 548
Izotov Y. I., Schaerer D., Worseck G., Guseva N. G., Thuan T. X., Verhamme A., Orlitová I., Fricke K. J., 2018a, *MNRAS*, 474, 4514
Izotov Y. I., Worseck G., Schaerer D., Guseva N. G., Thuan T. X., Fricke K. J., Verhamme A., Orlitová I., 2018b, *MNRAS*, 478, 4851
Jaskot A. E., Oey M. S., 2013, *ApJ*, 766, 91
Jaskot A. E., Oey M. S., 2014, *ApJ*, 791, L19
Jaskot A. E., Oey M. S., Scarlata C., Dowd T., 2017, *ApJ*, 851, L9
Jiang L. et al., 2018, *ApJ*, 772, 99
Kashikawa N. et al., 2011, *ApJ*, 734, 119
Kauffmann G. et al., 2003, *MNRAS*, 341, 33
Kennicutt R. C., Jr., 1998, *ARA&A*, 36, 189
Khairé V., Srianand R., Choudhury T. R., Gaikwad P., 2016, *MNRAS*, 457, 4051
Kimm T., Blaizot J., Carel T., Michel-Danzac L., Katz H., Rosdahl J., Verhamme A., Haehnelt M., 2019, *MNRAS*, 486, 2215
Kulkarni G., Worseck G., Hennawi J. F., 2019, *MNRAS*, 488, 1035
de La Vieuville G. et al., 2019, *A&A*, 628, 3
Leitherer C., Hernandez S., Lee J. C., Oey M. S., 2016, *ApJ*, 823, L64
Livermore R. C., Finkelstein S. L., Lotz, J. M., 2017, *ApJ*, 835, 113
Lodders K., 2003, *ApJ*, 591, 1220
Madau P., Haardt F., 2015, *ApJ*, 813, L8
Maseda M. V. et al., 2018, *ApJ*, 865, L1
Matsuoka Y. et al., 2018, *ApJ*, 869, 150
McKinney J. H., Jaskot A. E., Oey M. S., Yun M. S., Dowd T., Lowenthal J. D., 2019, *ApJ*, 874, 52
Mitra S., Ferrara A., Choudhury T. R., 2013, *MNRAS*, 428, L1
Mitra S., Choudhury T. R., Ferrara A., 2018, *MNRAS*, 473, 1416
Naidu R. P., Forrest B., Oesch P. A., Tran K.-V. H., Holden B. P., 2018, *MNRAS*, 478, 791

- Nakajima K., Ouchi M., 2014, MNRAS, 442, 900
- Nakajima K., Fletcher T., Ellis R. S., Robertson B. E., Iwata I., 2018, MNRAS, 477, 2098
- Orlitová I., Verhamme A., Henry A., Scarlata C., Jaskot A., Oey M. S., Schaerer D., 2018, A&A, 616, 60
- Ouchi M. et al., 2008, ApJS, 176, 301
- Ouchi M. et al., 2009, ApJ, 706, 1136
- Papaderos P., Izotov Y. I., Thuan T. X., Noeske K. G., Fricke K. J., Guseva N. G., Green R. F., 2002, A&A, 393, 461
- Parsa S., Dunlop J.S., McLure R. J., 2018, MNRAS, 474, 2904
- Paulino-Afonso A. et al., 2018, MNRAS, 476, 5479
- Rivera-Thorsen T. E. et al., 2017, A&A, 608, L4
- Rivera-Thorsen T. E. et al., 2019, preprint arXiv:1904.08186
- Robertson B. E. et al., 2013, ApJ, 768, 71
- Robertson B. E., Ellis R. S., Furlanetto S. R., Dunlop J. S., 2015, ApJ, 802, L19
- Rutkowski M. G. et al., 2017, ApJ, 841, L27
- Schaerer D., Hayes M., Verhamme A., Teyssier R., 2011, A&A, 531, 12
- Schaerer D., Izotov Y. I., Verhamme A., Orlitová I., Thuan T. X., Worseck G., Guseva, N. G., 2016, A&A, 591, L8
- Shapley A. E., Steidel C. C., Strom A. L., Bogosavljević M., Reddy N. A., Siana B. Mostardi R. E., Rudie G. C., 2016, ApJ, 826, L24
- Smith B. M. et al., 2018, ApJ, 853, 191
- Sobral D., Matthee J., 2019, A&A, 623, 157
- Stasińska G., Izotov Y., Morisset C., Guseva N., 2015, A&A, 576, 83
- Steidel C. C., Bogosavljević M., Shapley A.E., Reddy N. A., Rudie G. C., Pettini M., Trainor R. F., Strom A. L., 2018, ApJ, 869, 123
- Storey P. J., Hummer D. G., 1995, MNRAS, 272, 41
- Vanzella E. et al., 2010, ApJ, 725, 1011
- Vanzella E. et al., 2012, ApJ, 751, 70
- Vanzella E. et al., 2015, A&A, 576, 116
- Vanzella E. et al., 2018, MNRAS, 476, L15
- Verhamme A., Orlitová I., Schaerer D., Hayes M., 2015, A&A, 578, 7
- Verhamme A., Orlitová I., Schaerer D., Izotov Y., Worseck G., Thuan T. X., Guseva N., 2017, A&A, 597, 13
- Wise J. H., Cen R., 2009, ApJ, 693, 984
- Wisotzki L. et al., 2016, A&A, 587, 98
- Wisotzki L. et al., 2018, Nature, 562, 229
- Worseck G., Prochaska J. X., Hennawi J. F., McQuinn M., 2016, ApJ, 825, 144
- Wright E. L., 2006, PASP, 118, 1711
- Yajima H., Choi J.-H., Nagamine K., 2011, MNRAS, 412, 411
- Yang H. et al., 2017a, ApJ, 844, 171
- Yang H., Malhotra S., Rhoads J. E., Leitherer C., Wofford A., Jiang T., Wang J., 2017b, ApJ, 838, 4

APPENDIX A: EMISSION-LINE FLUXES IN SDSS SPECTRA AND ELEMENT ABUNDANCES

This paper has been typeset from a TeX/L^AT_EX file prepared by the author.

Table A1. Extinction-corrected emission-line fluxes in SDSS spectra

Line	λ	$100 \times I(\lambda) / I(\text{H}\beta)^{\text{a}}$							
		0007+0226	0159+0751	0820+5431	0926+4504	1032+4919	1205+4551	1242+4851	1355+4651
[O II]	3727	24.1± 1.7	18.4± 1.8	28.0± 2.8	22.7± 2.0	25.0± 1.2	20.3± 1.2	20.3± 1.9	22.8± 1.6
H12	3750	2.3± 1.2	4.6± 1.6	7.6± 2.0	5.0± 1.3	3.9± 2.9	4.3± 0.7
H11	3771	4.5± 1.1	4.7± 1.5	6.8± 2.6	5.4± 1.3	4.6± 2.9	5.7± 0.8	...	4.8± 1.1
H10	3798	4.9± 1.1	7.2± 1.6	7.9± 2.2	6.5± 1.6	6.1± 2.8	6.9± 0.8	6.7± 1.2	8.8± 1.1
H9	3836	7.1± 1.1	8.6± 1.5	10.7± 2.2	6.5± 1.6	7.9± 3.3	8.6± 0.8	9.2± 1.3	9.9± 1.0
[Ne III]	3869	59.2± 3.1	58.1± 3.4	50.1± 3.8	47.5± 3.1	48.0± 2.0	28.2± 1.4	49.4± 3.1	53.6± 2.8
H8+He I	3889	20.2± 1.6	20.0± 1.9	21.0± 2.5	14.6± 2.1	14.9± 3.4	17.6± 1.1	24.2± 4.4	23.3± 1.6
H7+[Ne III]	3969	34.7± 2.1	34.0± 2.4	33.8± 3.5	29.8± 2.5	32.2± 4.0	27.2± 1.4	30.1± 3.4	38.4± 2.3
H δ	4101	26.7± 1.8	26.5± 2.0	31.7± 3.0	25.2± 2.2	25.8± 3.8	28.4± 1.4	28.8± 3.4	26.8± 1.8
H γ	4340	47.3± 2.6	47.5± 2.8	48.6± 3.5	44.0± 3.0	44.8± 4.5	47.5± 2.0	49.7± 4.4	48.3± 2.6
[O III]	4363	19.7± 1.4	22.2± 1.7	21.6± 2.3	19.8± 1.7	19.8± 1.0	13.3± 0.8	19.6± 1.7	20.7± 1.4
He I	4471	3.5± 0.8	4.2± 0.8	3.0± 1.4	4.4± 1.0	4.0± 0.4	4.3± 0.5	4.6± 1.1	3.0± 0.7
He II	4686	1.3± 0.6	1.4± 0.6	...	0.9± 0.7	1.2± 0.3	3.8± 0.5	2.2± 0.9	2.7± 0.6
H β	4861	100.0± 4.5	100.0± 4.8	100.0± 6.0	100.0± 5.2	100.0± 5.4	100.0± 3.7	100.0± 3.7	100.0± 4.5
[O III]	4959	260.0±10.5	213.2± 9.1	197.3±10.5	223.6±10.3	209.8± 7.1	136.2± 4.9	174.7± 8.0	197.2± 8.1
[O III]	5007	775.0±29.9	630.6±25.6	568.2±24.3	674.0±29.1	4.3± 0.4 ^b	413.1±14.1	501.9±20.1	599.4±23.2
He I	5876	10.7± 1.0	11.3± 1.0	7.6± 1.3	11.9± 1.2	12.0± 0.7	12.0± 0.7	9.9± 1.1	8.7± 0.9
[O I]	6300	0.5± 0.4	0.5± 0.4	0.9± 0.2	1.5± 0.3	0.5± 0.6	0.9± 0.4
[S III]	6312	0.9± 0.5	0.7± 0.4	...	0.9± 0.5	1.1± 0.7	0.6± 0.2	0.7± 0.6	1.2± 0.4
H α	6563	277.3±12.1	275.3±12.4	231.8±13.1 ^b	275.3±13.5	132.9± 5.6 ^b	274.7±10.3	272.0±14.5	273.2±11.8
[N II]	6583	1.1± 0.5	1.2± 0.4	...	1.6± 0.6	2.0± 0.3	5.1± 0.5	1.2± 0.5	0.6± 0.4
He I	6678	2.9± 0.5	2.3± 0.5	2.8± 0.9	2.9± 0.7	3.2± 0.4	2.8± 0.3	3.2± 0.7	3.2± 0.5
[S II]	6717	2.9± 0.5	1.3± 0.4	3.0± 0.9	3.2± 0.7	2.6± 0.3	1.1± 0.3	2.4± 0.6	2.3± 0.4
[S II]	6731	2.2± 0.5	1.3± 0.4	1.4± 0.8	2.5± 0.6	2.5± 0.3	1.3± 0.3	2.5± 0.6	2.6± 0.5
He I	7065	3.4± 0.6	6.7± 0.7	3.6± 0.9	7.6± 0.9	7.7± 0.5	7.7± 0.5	3.7± 0.7	2.8± 0.5
[Ar III]	7136	3.7± 0.6	2.0± 0.4	3.2± 0.8	2.7± 0.6	3.0± 0.3	1.8± 0.3	2.3± 0.6	2.6± 0.5
$C(\text{H}\beta)^{\text{c}}$		0.130	0.425	0.000	0.075	0.000	0.160	0.085	0.065
$\text{EW}(\text{H}\beta)^{\text{d}}$		258±7	322±9	335±12	328±10	444±27	483±9	360±10	269±7
$\text{EW}(\lambda 5007)^{\text{d}}$		2180±20	1964±22	2200±45	1819±22	19±7 ^b	1718±15	1531±35	1541±15
$\text{EW}(\text{H}\alpha)^{\text{d}}$		1131±19	1629±27	1335±37 ^b	1733±35	932±50 ^b	1981±23	2210±60	1644±27
$F(\text{H}\beta)^{\text{e}}$		46.6±1.2	37.4±1.0	20.2±0.7	29.0±0.9	109.0±1.8	90.3±1.6	33.0±1.0	44.1±1.1

^a $I(\lambda)$ and $I(\text{H}\beta)$ are emission-line fluxes, corrected for the extinction derived from the Balmer decrement of hydrogen lines.^bClipped line.^c $C(\text{H}\beta)$ is the extinction coefficient derived from the Balmer decrement of hydrogen lines.^dRest-frame equivalent width in Å.^e $F(\text{H}\beta)$ is the observed $\text{H}\beta$ flux density in 10^{-16} erg s⁻¹ cm⁻².

Table A2. Electron temperatures, electron number densities and element abundances in H II regions

Parameter	Galaxy			
	0007+0226	0159+0751	0820+5431	0926+4504
T_e ([O III]), K	17090±700	20510±960	21410±950	18470±970
T_e ([O II]), K	14980±570	15630±740	15610±830	15380±750
T_e ([S III]), K	15620±580	18610±880	19110±890	17140±810
N_e ([S II]), cm ⁻³	90±40	660±300	10±10	140±50
O ⁺ /H ⁺ ×10 ⁵	0.22±0.03	0.16±0.02	0.22±0.04	0.19±0.03
O ²⁺ /H ⁺ ×10 ⁵	6.23±0.65	3.43±0.41	2.86±0.46	4.55±0.58
O ³⁺ /H ⁺ ×10 ⁶	0.88±0.44	0.66±0.34	...	0.45±0.37
O/H×10 ⁵	6.54±0.65	3.66±0.42	3.08±0.47	4.79±0.58
12+log(O/H)	7.82±0.04	7.56±0.05	7.49±0.07	7.68±0.05
N ⁺ /H ⁺ ×10 ⁷	0.81±0.26	0.84±0.22	...	1.11±0.33
ICF(N) ^a	25.01	20.48	...	21.61
N/H×10 ⁶	2.02±0.78	1.71±0.50	...	2.40±0.81
log(N/O)	-1.51±0.17	-1.33±0.14	...	-1.30±0.16
Ne ²⁺ /H ⁺ ×10 ⁵	1.10±0.12	0.69±0.08	0.54±0.09	0.73±0.10
ICF(Ne) ^a	1.00	1.02	1.03	1.01
Ne/H×10 ⁵	1.10±0.13	0.71±0.09	0.56±0.10	0.74±0.10
log(Ne/O)	-0.77±0.07	-0.71±0.07	-0.74±0.10	-0.81±0.08
S ⁺ /H ⁺ ×10 ⁷	0.49±0.08	0.24±0.09	...	0.54±0.10
S ²⁺ /H ⁺ ×10 ⁶	0.40±0.21	0.20±0.11	...	0.32±0.19
ICF(S) ^a	3.21	2.56	...	2.53
S/H×10 ⁶	1.44±0.68	0.57±0.28	...	0.94±0.49
log(S/O)	-1.66±0.21	-1.81±0.22	...	-1.71±0.23
Ar ²⁺ /H ⁺ ×10 ⁷	1.39±0.22	0.56±0.13	0.86±0.23	0.87±0.20
ICF(Ar) ^a	2.28	2.03	1.56	2.09
Ar/H×10 ⁷	3.16±1.34	1.14±0.81	1.34±0.09	1.82±1.21
log(Ar/O)	-2.32±0.19	-2.51±0.31	-2.36±0.31	-2.42±0.29

Parameter	Galaxy			
	1032+4919	1205+4551	1242+4851	1355+4651
T_e ([O III]), K	19540±620	19500±790	21750±930	20340±950
T_e ([O II]), K	15570±460	15560±590	15590±870	15630±670
T_e ([S III]), K	18090±510	18260±660	19400±910	18560±790
N_e ([S II]), cm ⁻³	560±50	1090±580	770±170	1200±150
O ⁺ /H ⁺ ×10 ⁵	0.21±0.02	0.18±0.02	0.18±0.03	0.21±0.03
O ²⁺ /H ⁺ ×10 ⁵	3.66±0.28	2.48±0.24	2.45±0.34	3.30±0.36
O ³⁺ /H ⁺ ×10 ⁶	0.43±0.12	1.09±0.21	0.55±0.26	0.89±0.27
O/H×10 ⁵	3.92±0.28	2.77±0.24	2.68±0.34	3.59±0.36
12+log(O/H)	7.59±0.03	7.44±0.04	7.43±0.06	7.56±0.04
N ⁺ /H ⁺ ×10 ⁷	1.38±0.17	3.53±0.33	0.81±0.29	0.40±0.19
ICF(N) ^a	16.24	13.50	13.60	15.57
N/H×10 ⁶	2.25±0.31	4.77±0.50	1.10±0.42	0.63±0.34
log(N/O)	-1.24±0.07	-0.76±0.06	-1.39±0.18	-1.76±0.24
Ne ²⁺ /H ⁺ ×10 ⁵	0.64±0.05	0.37±0.04	0.52±0.07	0.65±0.07
ICF(Ne) ^a	1.03	1.04	1.04	1.03
Ne/H×10 ⁵	0.66±0.05	0.40±0.04	0.54±0.09	0.68±0.08
log(Ne/O)	-0.77±0.05	-0.85±0.06	-0.70±0.08	-0.73±0.07
S ⁺ /H ⁺ ×10 ⁷	0.48±0.05	0.24±0.06	0.48±0.13	0.49±0.10
S ²⁺ /H ⁺ ×10 ⁶	0.32±0.07	0.17±0.07	0.16±0.14	0.32±0.11
ICF(S) ^a	2.03	2.37	2.45	2.17
S/H×10 ⁶	0.74±0.15	0.47±0.16	0.52±0.35	0.81±0.25
log(S/O)	-1.72±0.09	-1.77±0.16	-1.72±0.30	-1.65±0.14
Ar ²⁺ /H ⁺ ×10 ⁷	0.88±0.10	0.54±0.08	0.62±0.16	0.74±0.14
ICF(Ar) ^a	1.78	1.62	1.63	1.74
Ar/H×10 ⁷	1.57±0.39	0.87±0.34	1.01±0.70	1.28±0.59
log(Ar/O)	-2.40±0.11	-2.50±0.17	-2.43±0.31	-2.45±0.21

^aICF is the ionization correction factor.